Fall 2022

Assessing the Mechanics of Two Earthquake Clusters in the Basin and Range Province

Jamie Hansen
Central Washington University, jado8801@gmail.com

ASSESSING THE MECHANICS OF TWO EARTHQUAKE CLUSTERS IN THE BASIN AND RANGE PROVINCE

_____

A Thesis

Presented to

The Graduate Faculty

Central Washington University

_____

In Partial Fulfillment

of the Requirements for the Degree

Master of Science

Geological Sciences

_____

by

Jamie Michele Hansen

November 2022

CENTRAL WASHINGTON UNIVERSITY

Graduate Studies

We hereby approve the thesis of

Jamie Michele Hansen

Candidate for the degree of Master of Science

APPROVED FOR THE GRADUATE FACULTY

_____ _____
Dr. Walter Szeliga, Committee Chair

_____ _____
Dr. Breanyn MacInnes

_____ _____
Dr. Timothy Melbourne

_____ _____
Dean of Graduate Studies

ABSTRACT

ASSESSING THE MECHANICS OF TWO EARTHQUAKE CLUSTERS IN THE BASIN AND RANGE PROVINCE

by

Jamie Michele Hansen

November 2022

The seismicity in the Basin and Range Province of the western United States often manifests as clusters of earthquakes occurring over brief windows of time, lasting from months to years. Two different earthquake clusters occurring between 2014 and 2018, near Challis, Idaho and northwestern Nevada, were assessed in this study. The seismic activity in the southeastern section of the Challis cluster began with a M5.2 earthquake that was likely the main-shock earthquake in an aftershock sequence. The northwestern section of the Challis cluster does have several potential candidates for a main-shock earthquake, but none have been identified as a start to a true aftershock sequence, and there is no distinct spatial progression noted. Similarly, the Sheldon cluster also does not have a distinct spatial progression or main-shock earthquake. Using the classification method described by Vidale and Shearer in their 2006 paper, I analyzed the statistical, temporal, and spatial characteristics of both clusters to see how these two clusters compare. For the Challis region, the two sections of the cluster appear to have different driving mechanisms. While the northwest cluster falls under the “average” classification, the southeast cluster is categorized as “aftershock-like” sequence, suggesting that the southeast cluster is related to the Lost River Fault System. The

northwest cluster's seismicity may be due to hydrothermal activity, as there are several hot springs in the area. The Sheldon cluster, whose hypocentral distribution resembles a tube or a ball when mapped in 3D, falls under the classification of "swarm-like." The driving mechanism for this cluster is more difficult to determine, as there is no history of seismicity in this area, though there is some history of relatively recent magmatism and some currently active hot springs.

ACKNOWLEDGMENTS

I would like to thank Central Washington University for giving me the opportunity to pursue this degree and for providing me with financial assistance through a teaching assistantship and a summer fellowship. Thank you to the American Federation of Mineralogical Societies for additional funding for this project.

I would like to thank my committee members, Bre MacInnes and Tim Melbourne, for your guidance and mentorship over the course of this project, and for some of my favorite classes here at CWU. I am beyond grateful to my committee chair, Walter Szeliga, for your infinite amount of help, support, and patience, without which, I would not have been able to complete this project.

I would also like to thank my friends and family. Thank you to my parents for their steadfast encouragement and support. I could not have achieved my goals without you. Thank you to my fellow CWU students for your friendship, comradery, and some really great memories. Thank you to my friend Meaghan Wetherell, for your unwavering support, advice, and encouragement. Thank you for always being there.

TABLE OF CONTENTS

LIST OF TABLES

LIST OF FIGURES

LIST OF FIGURES (CONTINUED)

LIST OF FIGURES (CONTINUED)

CHAPTER I

INTRODUCTION

The Basin and Range Province is an area of general crustal extension, located in the western United States and Northern Mexico. This extension is the source of the active seismicity in the area, often seen as clusters of earthquakes that occur during a limited period of time. For this project, I have analyzed two different earthquake clusters, one located near Challis, Idaho, and the other in northwestern Nevada, near the Charles Sheldon National Antelope Refuge. The Challis cluster actually consists of at least two spatially distinct areas of seismic activity, with a northwesterly linear trend. In the southeast section of the Challis study area, this trend coincides with the northern extent of the fault that ruptured during the 1983 M7.3 Borah Peak earthquake. Aftershocks during the months following the 1983 Borah Peak earthquake also occurred along a similar northwesterly linear trend. In contrast, though the northwestern section of the Challis cluster does have several events larger than M4, making them potential candidates for a main-shock earthquake, none stand out as a start to a true aftershock sequence. There is also no distinct spatial progression noted for the northwest section of the Challis cluster. Similarly, the Sheldon cluster does not have a distinct spatial progression or main-shock earthquake.

Several studies have attempted to classify earthquake clusters and determine the driving force behind them, which allows for comparison of more recent events, with the goal of determining their origins and mechanics (Vidale and Shearer, 2006; Farrell et al., 2009; Ruhl et al., 2010; Brumbaugh et al., 2014). These studies are all similar in their classifications of earthquake clusters, but I have used the specific terminology and method from the Vidale and

Shearer classification (2006) in this project to analyze the statistical, temporal, and spatial characteristics of both clusters to determine the driving mechanism for the cluster activity.

It has been suggested by a number of papers that it is possible to see the difference between earthquake clusters from volcanic origins and clusters of tectonic origins (Vidale and Shearer, 2006; Farrell et al., 2009; Ruhl et al., 2010; Brumbaugh et al., 2014). Though these papers assessed earthquake clusters of both volcanic and tectonic origins, each assessed clusters in an area in which one was more likely than the other. For instance, Vidale and Shearer (2006) looked at clusters in southern California, which is an area much more likely to have clusters of tectonic origin, whereas Farrell et al. (2009) assessed clusters in the Yellowstone area, which would be much more likely to have a volcanic origin. The Basin and Range Province is an area in which earthquake clusters from both origins can be found. As such, the purpose of my research is to use the information from previous studies, comparing their methods and results, to classify these two earthquake clusters in the Basin and Range Province.

CHAPTER II

BACKGROUND

Geologic Setting of the Basin and Range Province

Named for its distinctive topography of alternating basins and ranges, the Basin and Range Province (BRP) is larger than most continental rifts at greater than 900km across, at its widest point (Parsons, 1995). Other similarly large rift basins, such as the East African Rift, are located below sea level, unlike the BRP which has an average elevation of approximately 1.5km above sea level. Dividing the province into the northern, central, and southern Basin and Range not only separates the area geographically, but also by general tectonic trends. The northern BRP is comprised of two large-offset, high-angle normal fault systems, the Sevier Desert and the Snake River detachment systems, located in western Utah and southwestern Idaho respectively. The central BRP consists of additional normal fault systems, as well as some distinct strike-slip elements. The southern BRP is noted for the extension of its metamorphic core complexes, which were formed by large-offset normal fault systems (McQuarrie and Wernicke, 2005). This widespread faulting and extension both contribute to the active seismicity within the area. The two earthquake clusters assessed in this study are both located in the northern BRP, in areas of geologically recent magmatism (Figure 2).

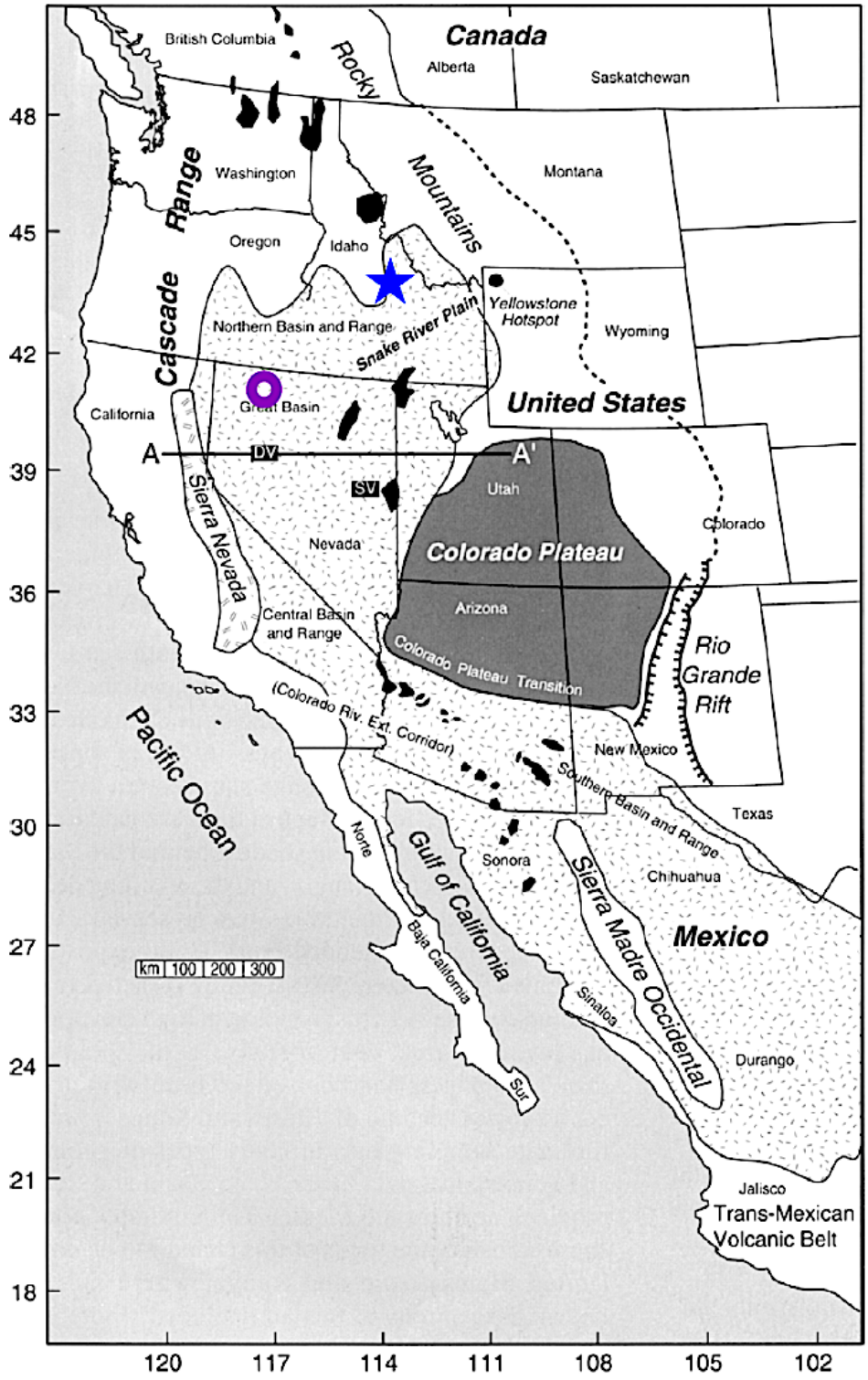

Figure 1: Edited map of the Basin and Range Province. The area with the stippled pattern marks the constraints of the BRP. The black areas are metamorphic core complexes. The blue star represents the Idaho cluster, and the purple circle represents the Nevada cluster. Figure from Parsons (1995).

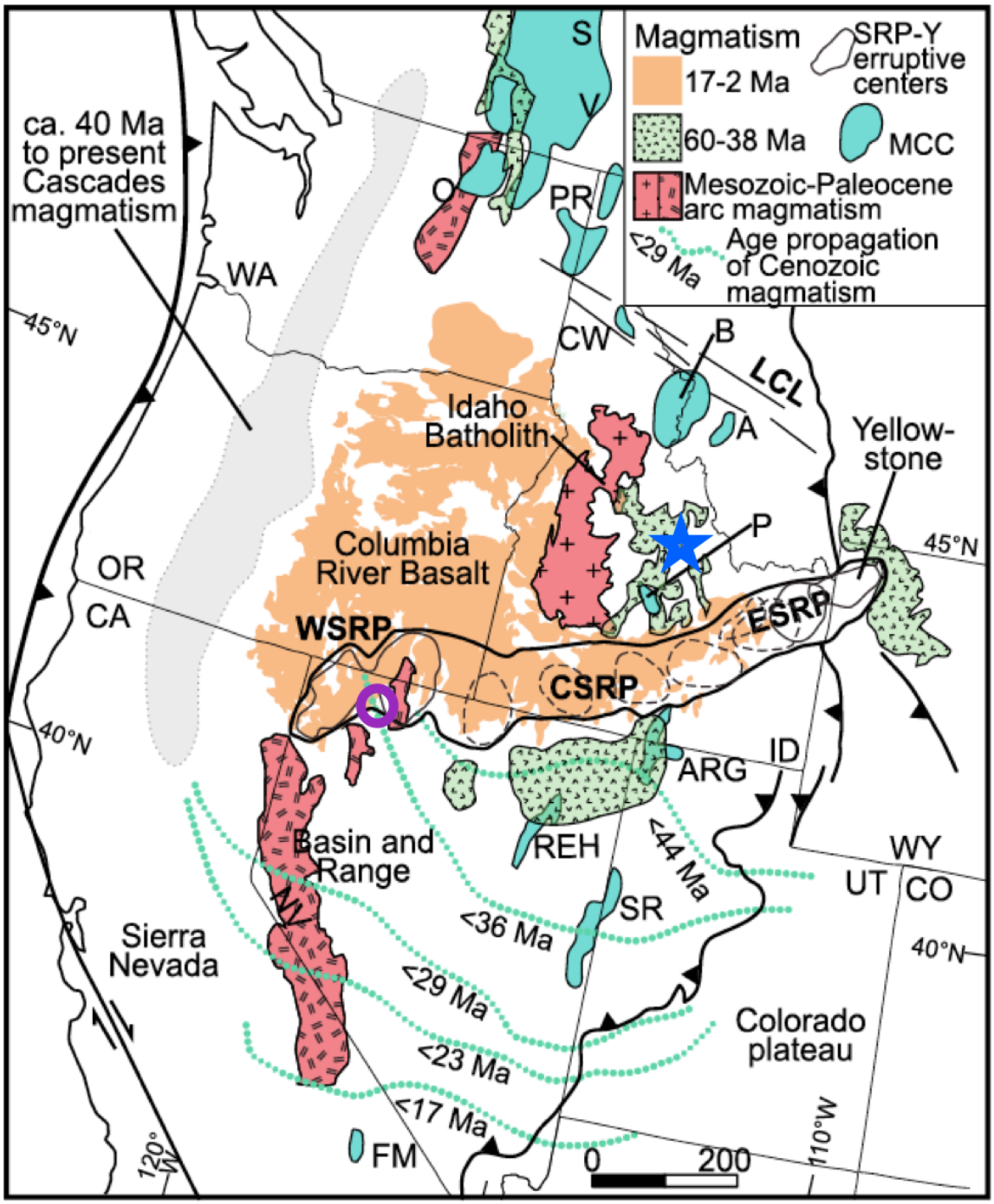

Figure 2: Edited map of the Basin and Range area highlighting magmatic suites and metamorphic core complexes (MCC). ESRP = Eastern Snake River Plain, CSRP = Central Snake River Plain, WSRP = Western Snake River Plain, LCL = Lewis and Clark shear zone. Core complexes: S = Shuswap, V = Valhalla, O = Okanogan, PR = Priest River, CW= Clear Water, B = Bitterroot, A = Anaconda, P = Pioneer, ARG = Albion-Raft River-Grouse Creek, REH = Ruby-East Humboldt, SR = Snake Range, and FM = Funeral Mountains. The blue star represents the Idaho cluster, and the purple circle represents the Nevada cluster. Figure from Konstantinou and Miller (2015).

Earthquake Clusters near Challis, Idaho

The region around Challis, ID is distinguished in particular by its background seismicity, with a few earthquakes per year and magnitudes up to 5.6 (USGS, 2016). In January of 2014, an earthquake cluster began near Challis, Idaho, concluding in December of 2014. A second cluster began in January of 2015 to the southeast of this first cluster. Though it occasionally had periods of diminished activity, the cluster continued until May of 2017. Most of the earthquakes in these clusters are of magnitude 2-3.5, with one as high as magnitude 5.2. The first of the two spatial clusters is located to the northwest of the town of Challis, Idaho and the second is located approximately 20km to the southeast, along a northwest linear trend line. The Lost River Fault is a high-angle, southwest-facing, segmented normal fault that is exposed along the west flank of the Lost River Range (IGS, 2016). In October of 1983, an approximately 36km long segment of the fault ruptured with an M_s of 7.3 (Richins et al., 1987). Aftershock sequences from this earthquake have been documented along the fault segments in the Lost River Fault System. In August of 1984, a late aftershock sequence from the 1983 Borah Peak earthquake occurred. This sequence has been called the Devil Canyon sequence after the location of the magnitude 5.8 earthquake that started the sequence (Payne et al., 2004). 237 events were recorded between the surface expressions of the Lost River and the Lone Pine faults. The events started along the Challis segment of the Lost River Fault System, but after a magnitude 5.0 event in September of 1984, the sequence shifted closer to the Lone Pine Fault (Figure 3). In addition to its seismicity, the Challis area has a history of geologically recent magmatism. Exposed 13 miles northwest of Challis are large volcanic fields, including the Van

Horn caldera complex and the Twin Peaks caldera. These volcanic fields were active between about 51-40Ma, ranging from mafic to rhyolitic flows (Moye et al., 1988).

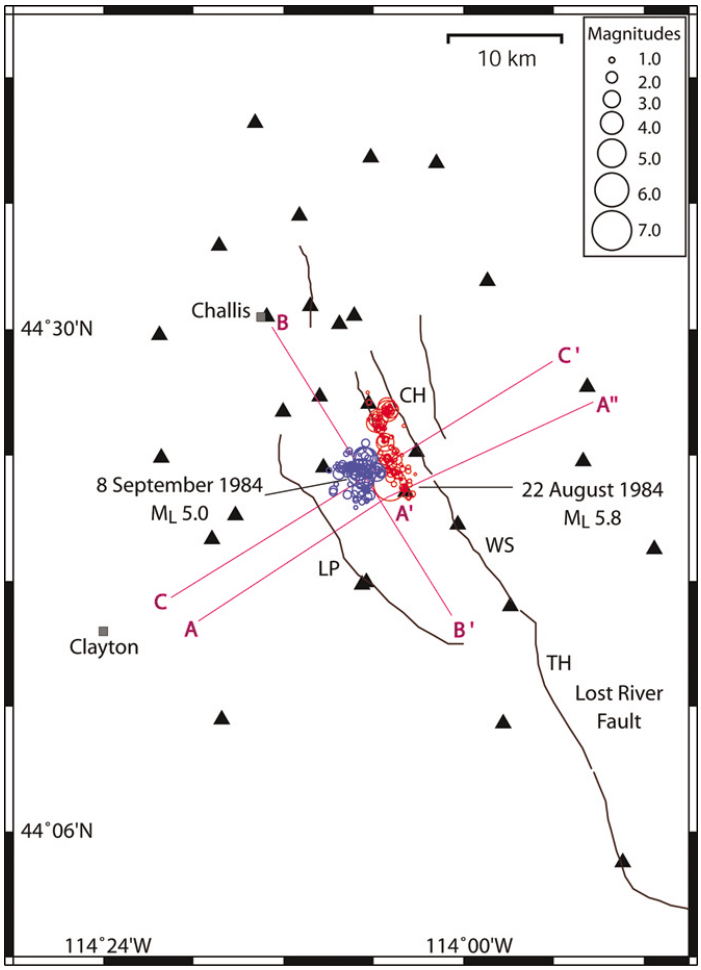

Figure 3: Locations of the temporary seismic stations (black triangles) for the 1984 Devil Canyon earthquake survey. Hypocenters associated with the Challis Segment are shown as red circles, and those associated with the Lone Pine fault are shown as blue circles. Cross sections A-A' and C-C' are perpendicular to the N39°W strike of the Lone Pine fault, and A'-A" is perpendicular to the N25°W strike of the central strand of the Challis segment. The Lone Pine fault is labeled LP and the northern segments of the Lost River fault are labeled CH, Challis; WS, Warm Springs; and TH, Thousand Springs. Figure from Payne et al. (2004).

Earthquake Cluster near Sheldon Wildlife Refuge, Nevada

The Sheldon cluster is located in a very remote area containing only the Sheldon National Wildlife Refuge and differs from the Challis cluster in several ways. Prior to the start of the swarm in July of 2014, there had been no noted seismicity documented in this particular

region of Nevada (USGS, 2016). There have been seven earthquakes in the area around the Refuge since 1900, but they were not recorded in the same area as the current cluster. Additionally, a small cluster of about 30 events occurred in July of 2007 approximately 20 miles northwest of the refuge. The Sheldon cluster has a significantly larger total number of earthquakes, with 7191 events, as compared to 751 for the Challis cluster. The two clusters are notably comparable in magnitude, but the Sheldon cluster lacks an obvious spatial pattern. Similar to the Challis cluster, the area of the Sheldon cluster has a history of geologically recent magmatism, though very little geologic information is available regarding the Sheldon-Antelope Volcanic Field. The monogenetic volcanic field consists of 3 to 4 basalt flows from small shield volcanoes. One geochronologic result of 1.2 ± 0.5 Ma indicates this is a young volcanic field (Wood, 1990).

CHAPTER III

METHODS

Classification

Several studies have categorized, classified, and analyzed the mechanics of earthquake swarms and aftershock sequences (e.g. Vidale and Shearer, 2006; Farrell et al., 2009; Ruhl et al., 2010; Brumbaugh et al., 2014). Some of these suggested it is possible to determine the difference between clusters whose driving mechanism is volcanic as opposed to tectonic. All of the classification systems were similar, but the classification system used by Vidale and Shearer (2006) was the focus in the classification of the Challis and Sheldon clusters in this work, as that method was described in more detail and covered a greater range of variables. In general, swarm activity can be categorized through the spatial and temporal progression of earthquakes along a planar surface. Where no mapped faults are currently known, planar features may still be recovered from the earthquake locations using a technique called principal component analysis, which is a way of condensing data into orthogonal planes. Some earthquake swarms do not display a clear main-shock/aftershock pattern, but are perceived to show a lateral or radial progression. In the classification scheme of Vidale and Shearer (2006), these clusters are called “swarm-like” (Figure 4), and are likely a result of pore-fluid pressure fluctuations over time based on the planes on which hypocenters were located and the pattern of progression, with aseismic slip as a possible contributing factor. Other clusters display a clear main-shock/aftershock pattern in which the largest magnitude event occurs first and subsequent events were smaller. In the classification scheme of Vidale and Shearer (2006), these clusters, termed “aftershock-like”, can reveal a progression trend as well (Figure 5). Some earthquake

clusters do not have any kind of trend or pattern. They do not present a clear main-shock/aftershock pattern or any kind of progression. In the classification scheme of Vidale and Shearer (2006), these clusters are called “average” (Figure 6).

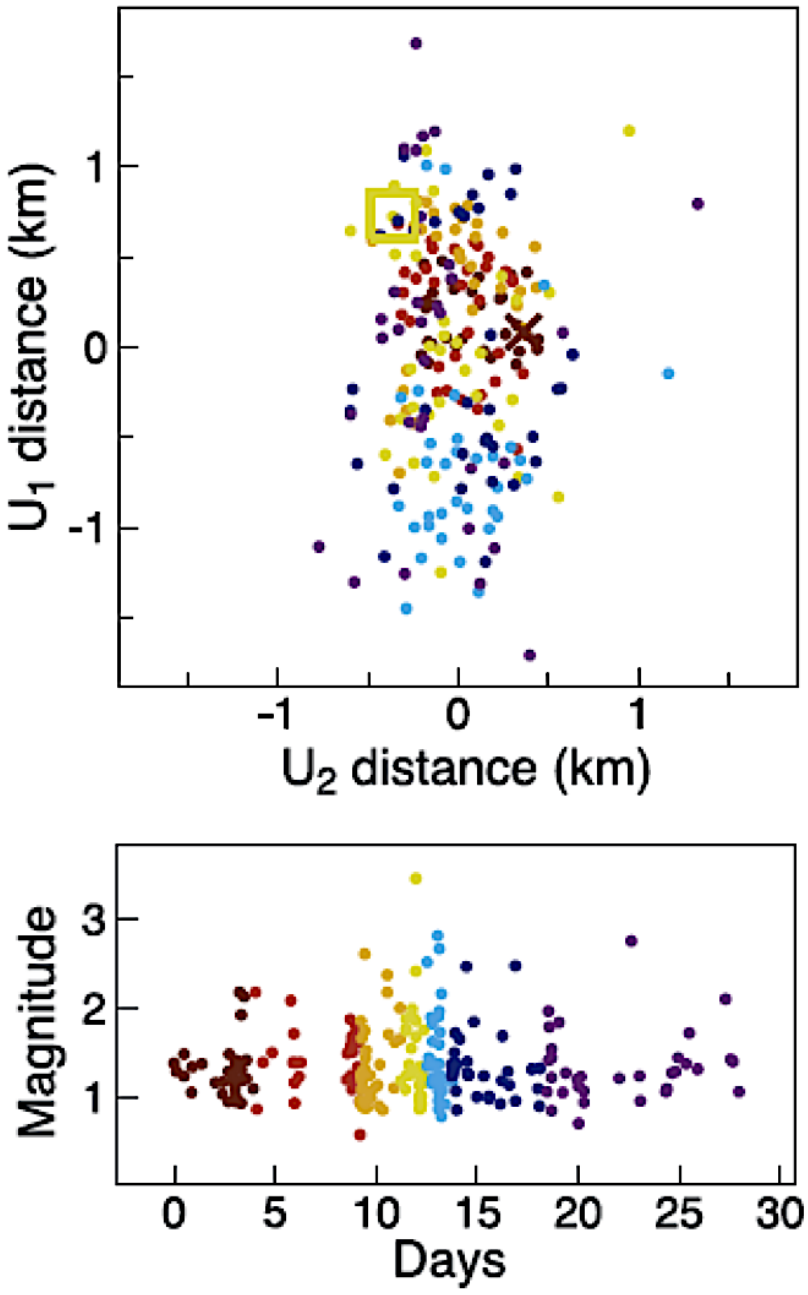

Figure 4: Data from an example of a “swarm-like” seismic burst, located near Ontario, California, beginning in July of 1994. There are 230 events at 5km depth. The different colors represent 7 different time periods, each of a few days. The cross represents the first event and the square is the event of largest magnitude. Figure from Vidale and Shearer (2006).

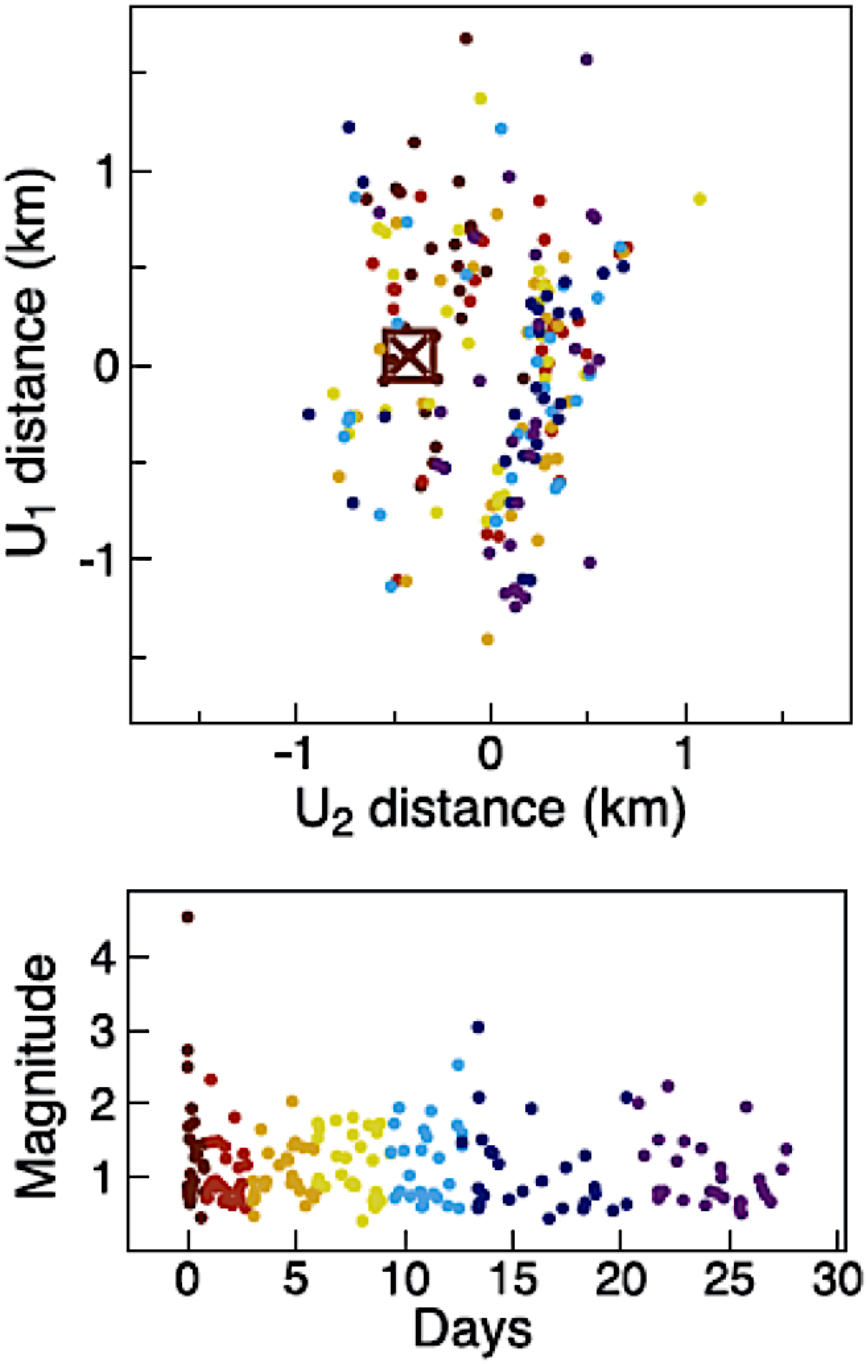

Figure 5: Data from an example of an "aftershock-like" seismic burst, located near Grapevine Mountain, California, beginning in October of 1984. There are 190 events at 9km depth. The different colors represent 7 different time periods, each of a few days. The cross represents the first event and the square is the event of largest magnitude, which in this case, is the same event. Figure from Vidale and Shearer (2006).

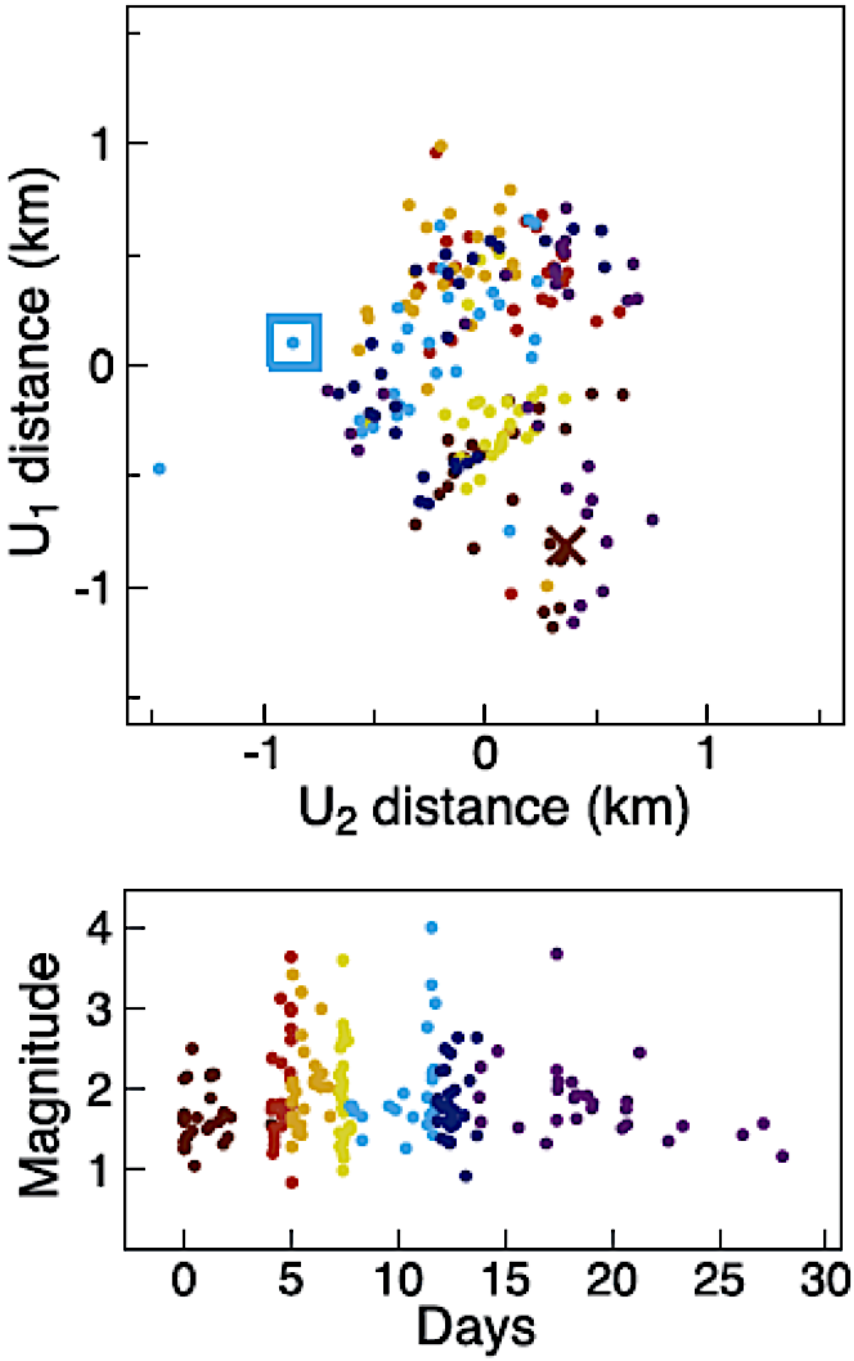

Figure 6: Data from an example of an "average" seismic burst, located near Pushawalla Canyon, California, beginning in April of 1990. There are 189 events at 3km depth. The different colors represent 7 different time periods, each of a few days. The cross represents the first event and the square is the event of largest magnitude. This burst differs from the "swarm-like" burst in that there is no migration trend. Figure from Vidale and Shearer (2006).

In areas with few seismic stations, the location of earthquake hypocenters is more difficult to precisely determine with standard earthquake location methods, meaning that any pattern or spatial progression of the hypocenters would also be difficult to assess. Previous studies have shown that the cross-correlation of seismic waveforms can be used to enhance accuracy of earthquake locations and provide first-order constraints on the spatial progression of an earthquake swarm (Ruhl et al., 2010).

It can also be difficult to determine the cause of an earthquake cluster. The frequency-magnitude distribution graph of the earthquakes in a cluster generally shows a decreasing trend in the number of earthquakes with increasing magnitude (Figure 7). This decreasing trend is known as the Gutenberg-Richter law. Previous studies have suggested that the slope of this graph, called the b-value, provides insight into the stress environment of the region (Farrell et al., 2009; Ruhl et al., 2010; Brumbaugh et al., 2014). Higher b-values (>1) are generally associated with areas of higher thermal gradient, such as areas with migrating magma or hydrothermal fluids, resulting in lower stress environments, while lower b-values (<1) are associated with higher stress environments (Farrell et al., 2009).

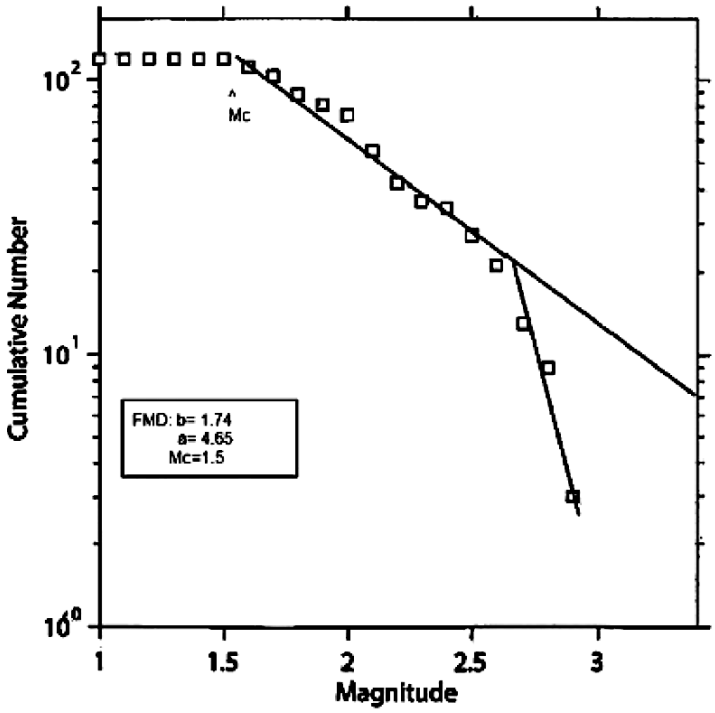

Figure 7: Frequency-Magnitude distribution of 2009 Sunset Crater earthquake swarm. An elevated b-value of 1.74 was calculated. Figure from Brumbaugh et al. (2014).

While the Gutenberg-Richter Law displays the trend in the frequency and magnitude of earthquakes in a cluster, the Omori Law and the modified Omori Law provides a prediction in the frequency of earthquakes over time. The Omori Law and the modified Omori Law have been used in the analysis of numerous aftershock sequences. Utsu et al. (1995) provides a comprehensive summary of many of these studies. The Omori Law was originally proposed in 1894 as a way of explaining the decay of aftershocks over time. Represented as $n(t) = K(t+c)^{-1}$, $n(t)$ is the frequency of aftershocks with respect to time t, with K and c as constants. Utsu proposed the modified Omori Law, $n(t) = K(t+c)^{-p}$, in 1957. The p value represents a decay parameter that varies with each sequence, found to be between 0.6–2.5, though most often between 0.9-1.5 (Utsu et al., 1995). While relocations and B-value estimates were utilized in

the classification of the Challis and Sheldon earthquake clusters, further analysis of these clusters using the modified Omori Law were not completed due to issues stemming from the sparse seismic network.

Challis and Sheldon Earthquakes

In January of 2014, a cluster of earthquakes began near the town of Challis, in central Idaho. The seismic events in this cluster continued until the end of 2014. In January of 2015, another cluster began approximately 20 km southeast of the 2014 cluster. As this area of Idaho is remote and there is sparse seismometer coverage, with the closest permanent seismometer located approximately 80 km away, local scientists deployed seven additional seismometers in the area from April to October of 2014. One of the seismometers in this temporary network was left active until July of 2015, at which time a new permanent seismometer was deployed in the area of the second cluster. In 2018, Pang et al. (2018) published an article on the Challis cluster based on data collected by these seismometers. As these additional seismometers provided a more complete catalog than the existing regional seismic network alone, the data from Pang et al. (2018) was used in this study. The events were relocated using a combination of the master event technique, the HYPOINVERSE program, and the GrowClust relocation algorithm (Pang et al., 2018). There are 751 total events in these two clusters and the maximum magnitude is 5.2.

In July of 2014, another cluster of earthquakes began near the Sheldon National Wildlife Refuge in northwestern Nevada. This cluster continued until May of 2018, with a total of 7,161 events, and a maximum magnitude of 4.7. There have been a couple of small additional

clusters in the area, one in September of 2020 and one in March of 2022. The data for the Sheldon cluster was obtained from the United States Geological Survey. HypoDD, a computer program that uses a double-difference algorithm was used to relocate the earthquakes in the catalog for the Sheldon cluster. The algorithm uses absolute time measurements, combined with time measurements from the cross correlation of P- and S-wave differentials for pairs of earthquakes observed at common seismic stations (Waldhauser and Ellsworth, 2000). The double-difference technique has been shown to linearize diffuse groupings of hypocenters, allowing for visualization of fault systems. The figures in the following chapter were produced using ZMAP, a software package available through Matlab, used to analyze earthquake catalogs. The latest version, v7, currently available as an alpha version, was used in this study.

CHAPTER IV

RESULTS AND DISCUSSION

Challis Clusters

When looking at the catalog (Pang et al., 2018) for the Challis sequence, the events begin in the northwest cluster, then the southeast cluster is active for a time, and then the events move back to the northwest cluster, with some sporadic events occurring outside of these two main clusters (Figure 8). While there is some spatiotemporal evolution, Vidale and Shearer (2006) described the swarm-like bursts to either spread outwards or move laterally from a point. The evolution seen in Figure 8 could be considered moving laterally, though Vidale and Shearer (2006) did not discuss any of their bursts as moving back and forth. The depth of the earthquakes in these clusters appear to be mostly between 6 and 10km for the northwest cluster and between 10 and 13km for the southeast cluster, as seen in Figure 9. The catalog for the Challis burst has a magnitude of completion of 1.8 and a b-value of 0.79 +/- 0.03, as seen in Figure 10.

The largest magnitude event (M5.2) did not occur first (magnitude >4 events are marked with stars in the figures), but about one year into the burst, on January 3rd, 2015. However, there were several M4+ earthquakes that occurred at the beginning of the burst. When looking at the cumulative number of earthquakes over time for this catalog (Figure 11), there is an obvious stair-step pattern noted, with three large steps standing out.

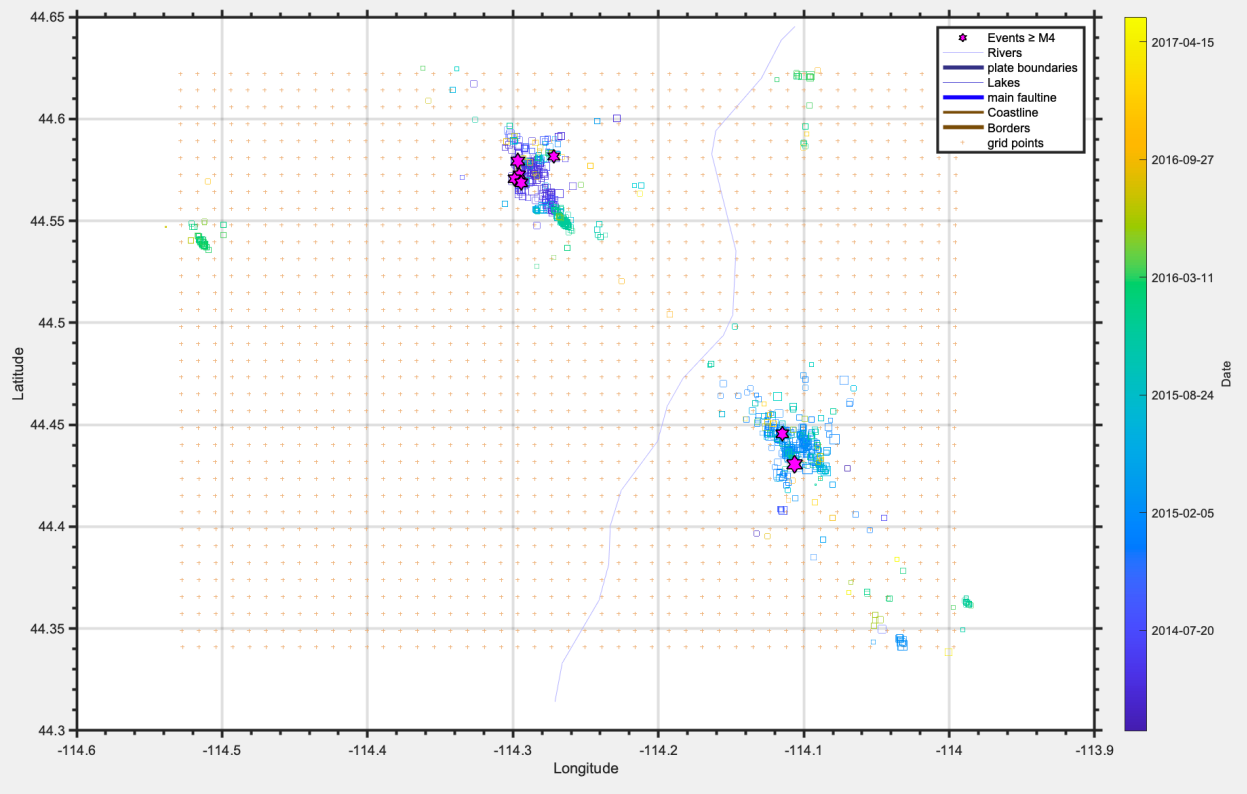

Figure 8: 2D map of the Challis data, color coded for time. Stars note earthquakes M4+. Blue line denotes a river in map-view.

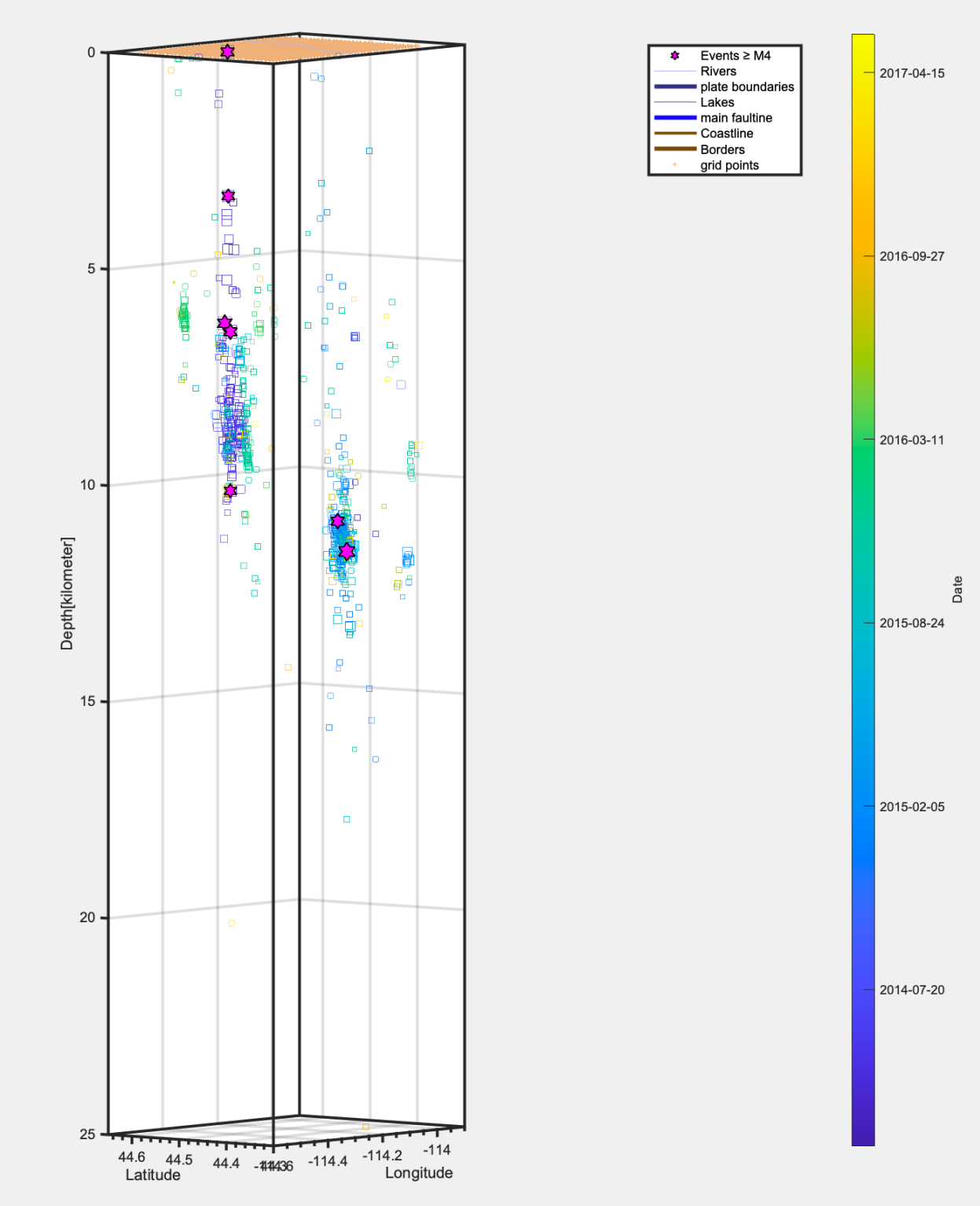

Figure 9: 3D plot of the Challis data, color coded for time. Stars note earthquakes M4+.

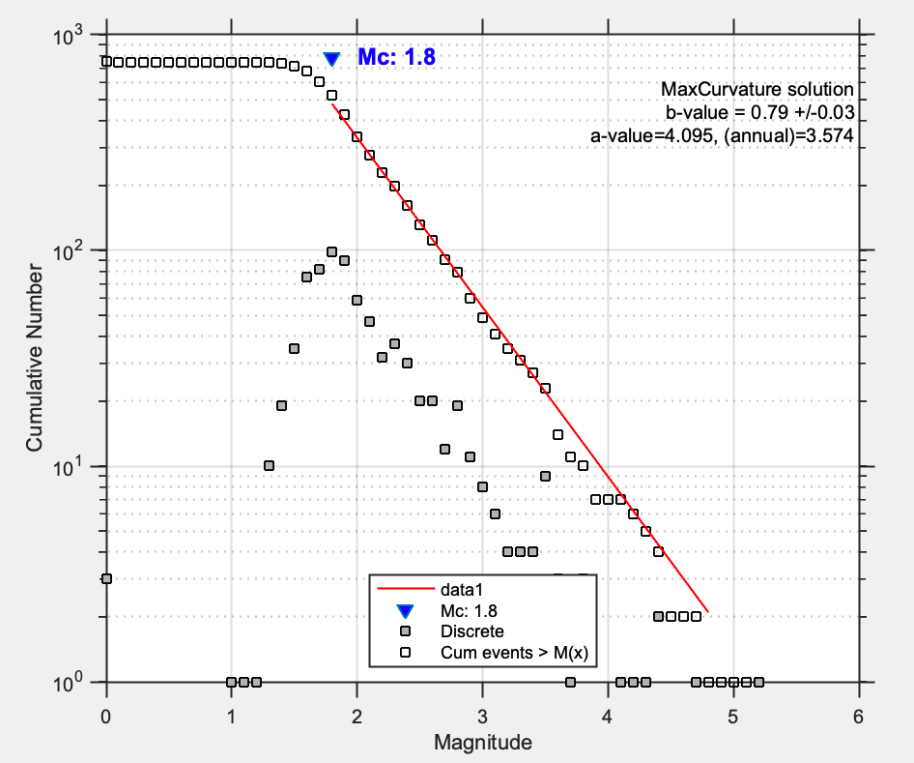

Figure 10: Frequency-Magnitude distribution of the Challis data. Mc is the magnitude of completeness, which is the minimum magnitude above which all of the earthquakes in the catalog are reliably detected.

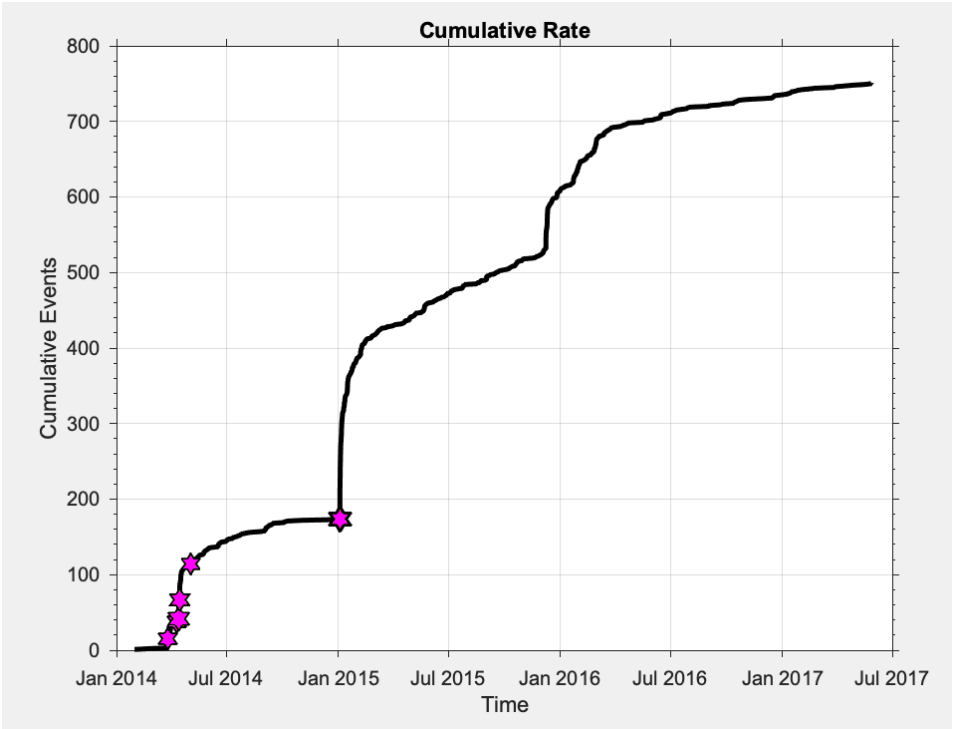

Figure 11: Cumulative earthquakes over time for the Challis data. Stars note earthquakes M4+.

Challis Clusters Defined Temporally

When looking at the cumulative earthquakes over time, there are three obvious groups of activity, seen as a stair-step pattern (Figure 11). The most logical cause for this pattern would be three separate bursts or sequences. The smaller steps seen within the three larger steps may be the result of a lower number of seismic stations in this area as compared to areas more frequently studied. Fewer seismic stations can result in incomplete datasets as earthquakes may be missed due to insufficient coverage, which would be seen as small steps in a plot of cumulative earthquakes over time.

Based on the dates of the three large steps, I separated the catalog into three groups. The first of these three groups is seen in Figures 12 – 15. There was a M4.2 earthquake on March 25th, 2014, a M4.3 on April 10th, 2014, a M4.7 on April 13th, 2014, a M4.4 on April 14th, 2014, and a M4.1 on May 3rd, 2014. As these are all larger events, there is no obvious mainshock earthquake to start an aftershock sequence. Nearly all of the events for this group occurred in the northwest cluster. When looking at the 3D plot of this group (Figure 13), the five larger magnitude earthquakes vary significantly in terms of depth. The M4.2 earthquake was at a depth of 3.4km, the M4.3 at 0.1km, the M4.7 at 6.4km, the M4.4 at 6.6km, and the M4.1 at 10.3km. There is some variation in the depth of the rest of the earthquakes in Group 1, but most occurred between 8 and 10km. Group 1 of the Challis data has a magnitude of completeness of 2.4 and a b-value of 0.91 +/- 0.10 (Figure 14). When looking at the cumulative earthquakes over time (Figure 15), this appears similar to that of an aftershock sequence, but there is more of a stepping pattern. The larger steps may be explained by the multiple larger magnitude earthquakes in this group, producing small aftershock sequences within the cluster.

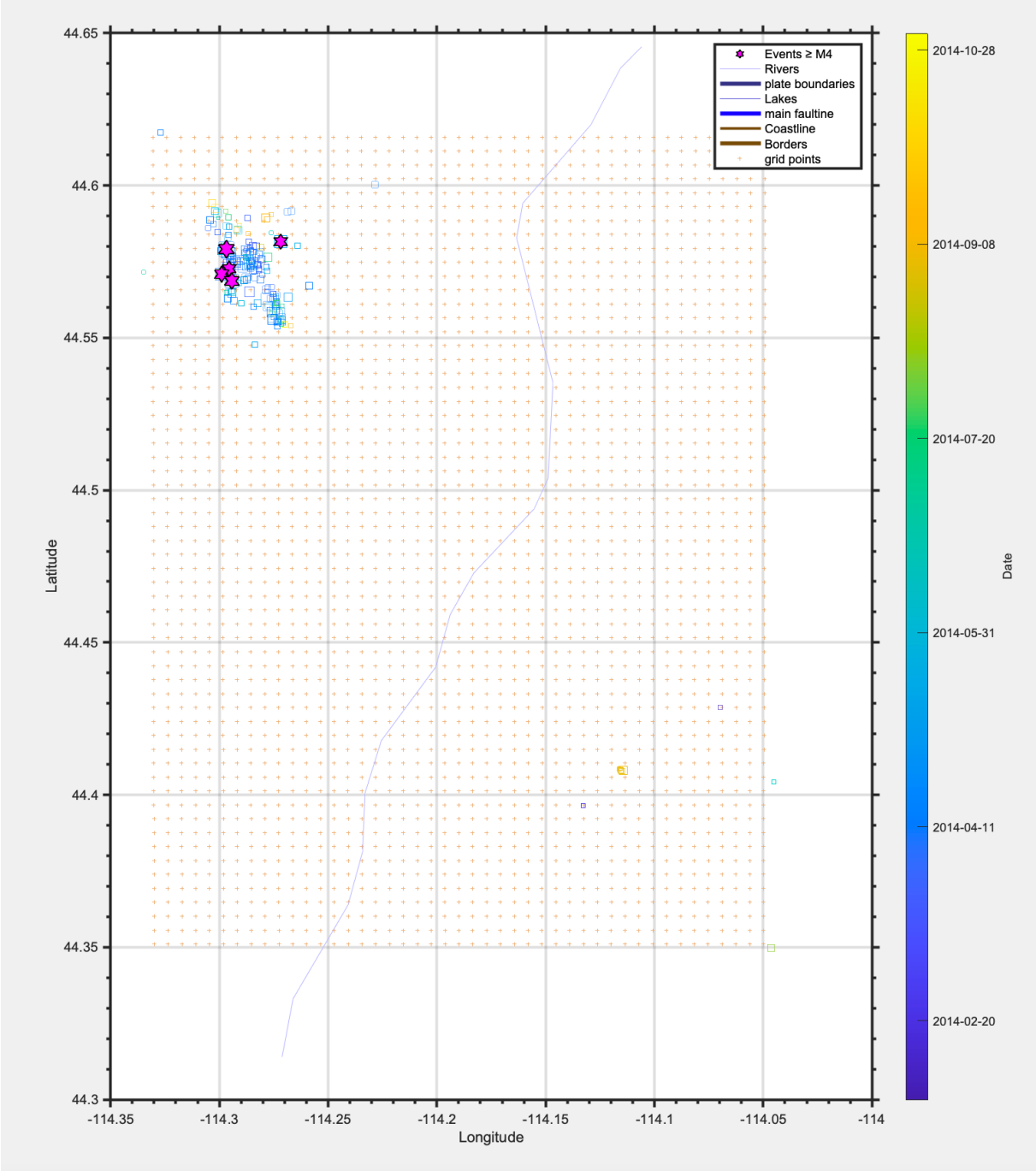

Figure 12: 2D map of Group 1 of the Challis data, color coded for time. Stars note earthquakes M4+. Blue line denotes a river in map-view.

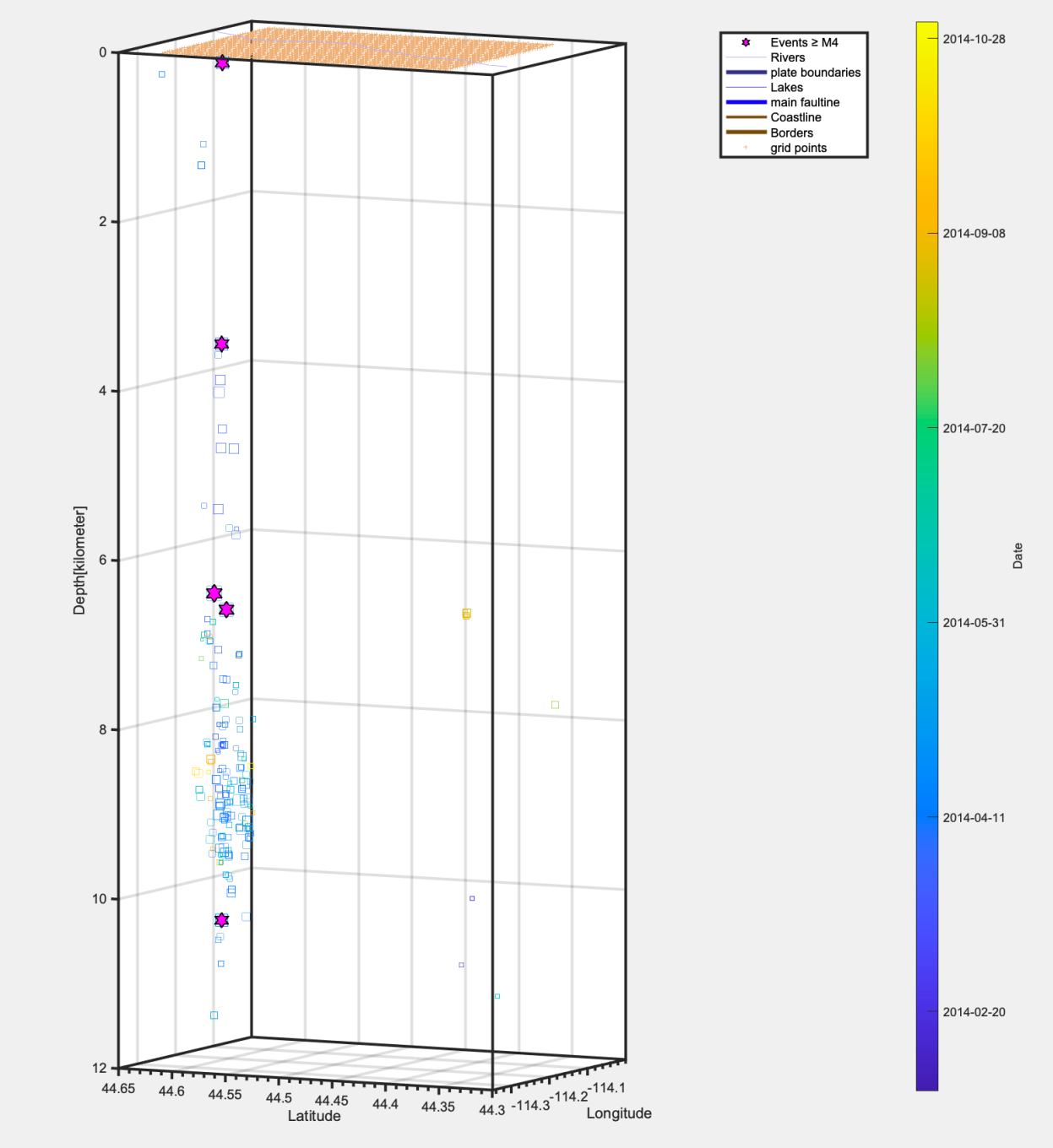

Figure 13: 3D plot of Group 1 of the Challis data, color coded for time. Stars note earthquakes M4+.

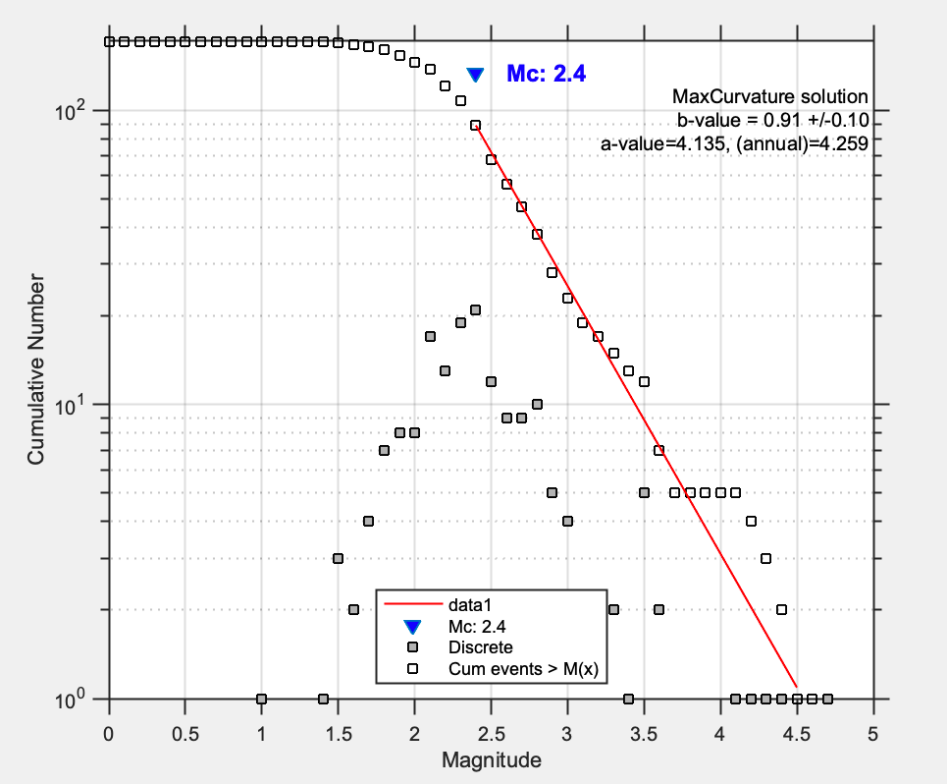

Figure 14: Frequency-Magnitude distribution of Group 1 of the Challis data.

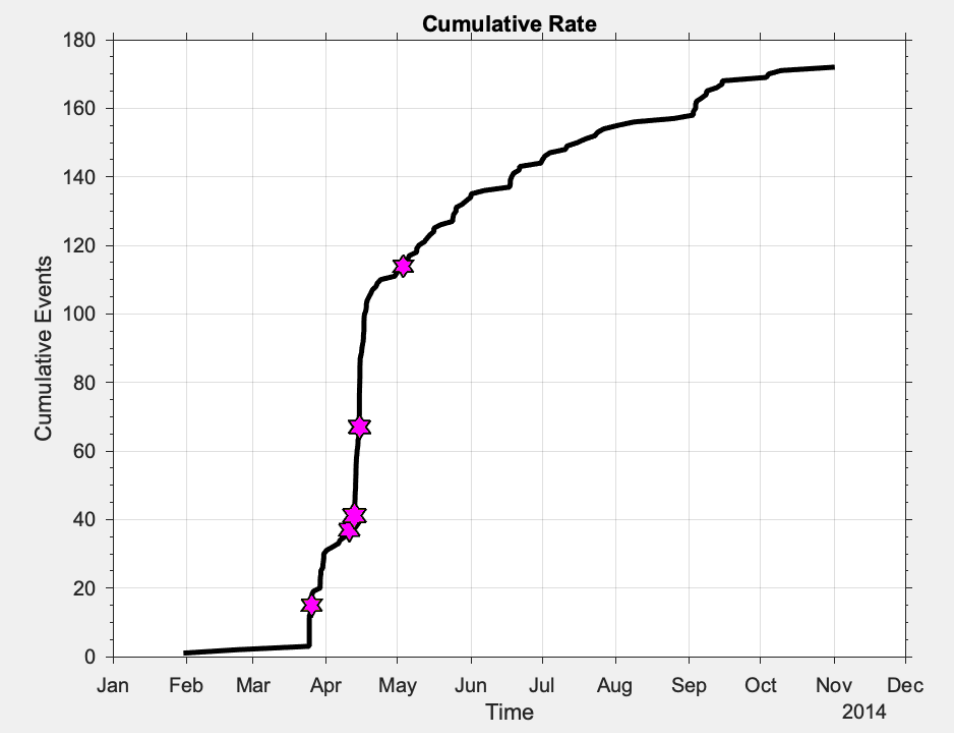

Figure 15: Cumulative earthquakes over time for Group 1 of the Challis data. Stars note earthquakes M4+.

Group 2 of the Challis data (Figures 16 – 19) begins with a 5.2 magnitude earthquake on January 3rd, 2015, immediately followed by a magnitude 4.4 earthquake, that occurred a little more than four minutes later. As seen in Figure 16, the group 2 earthquakes occurred mostly in the southeast cluster, with the majority occurring between 10 and 12km depth (Figure 17). Group 2 of the Challis data has a magnitude of completion of 1.8 and a b-value of 0.90 +/- 0.06 (Figure 18). The cumulative rate plot (Figure 19) is consistent with an aftershock sequence, with a small amount of stepping, likely due to lower coverage of seismic stations.

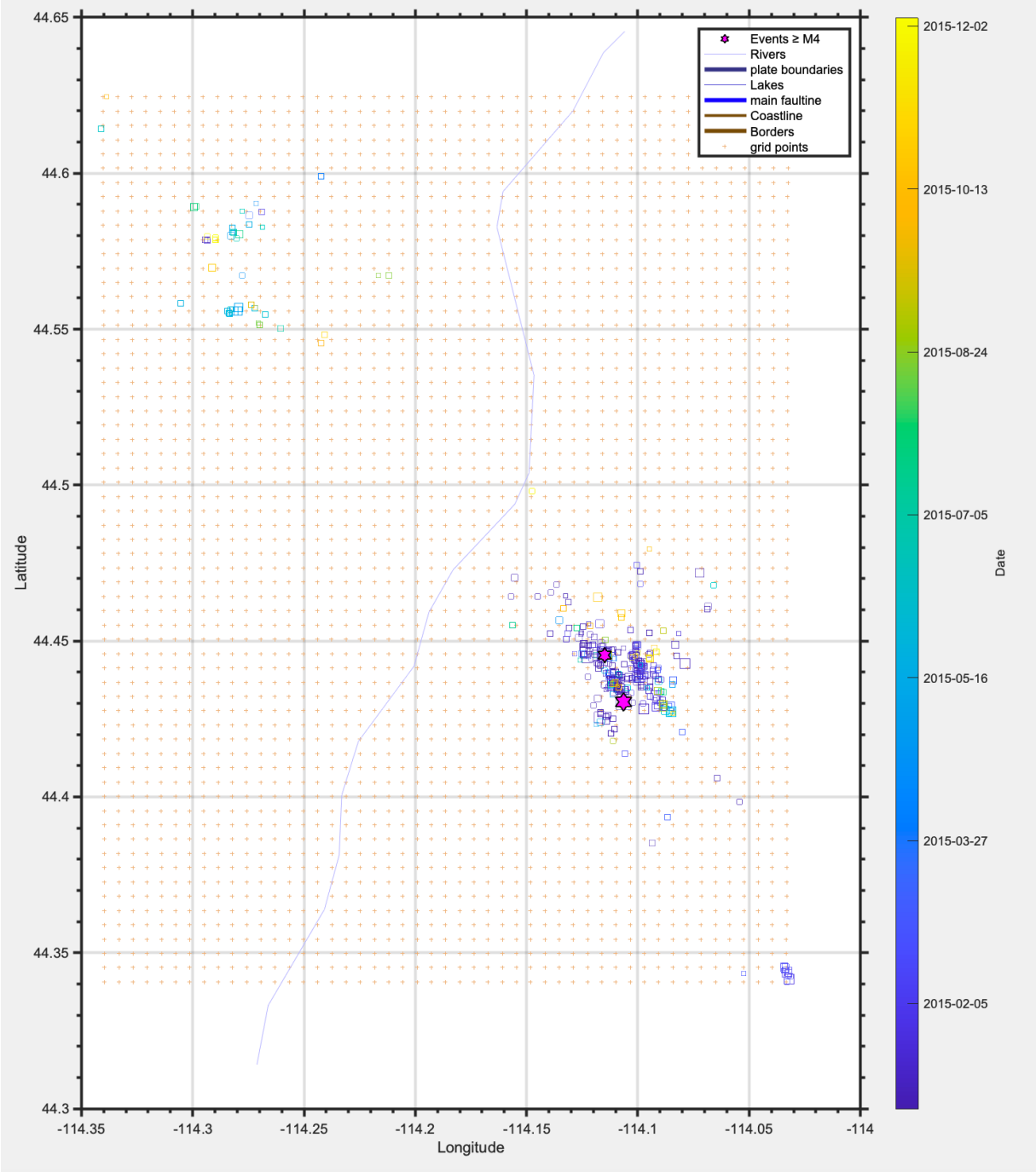

Figure 16: 2D map of Group 2 of the Challis data, color coded for time. Stars note earthquakes M4+. Blue line denotes a river in map-view.

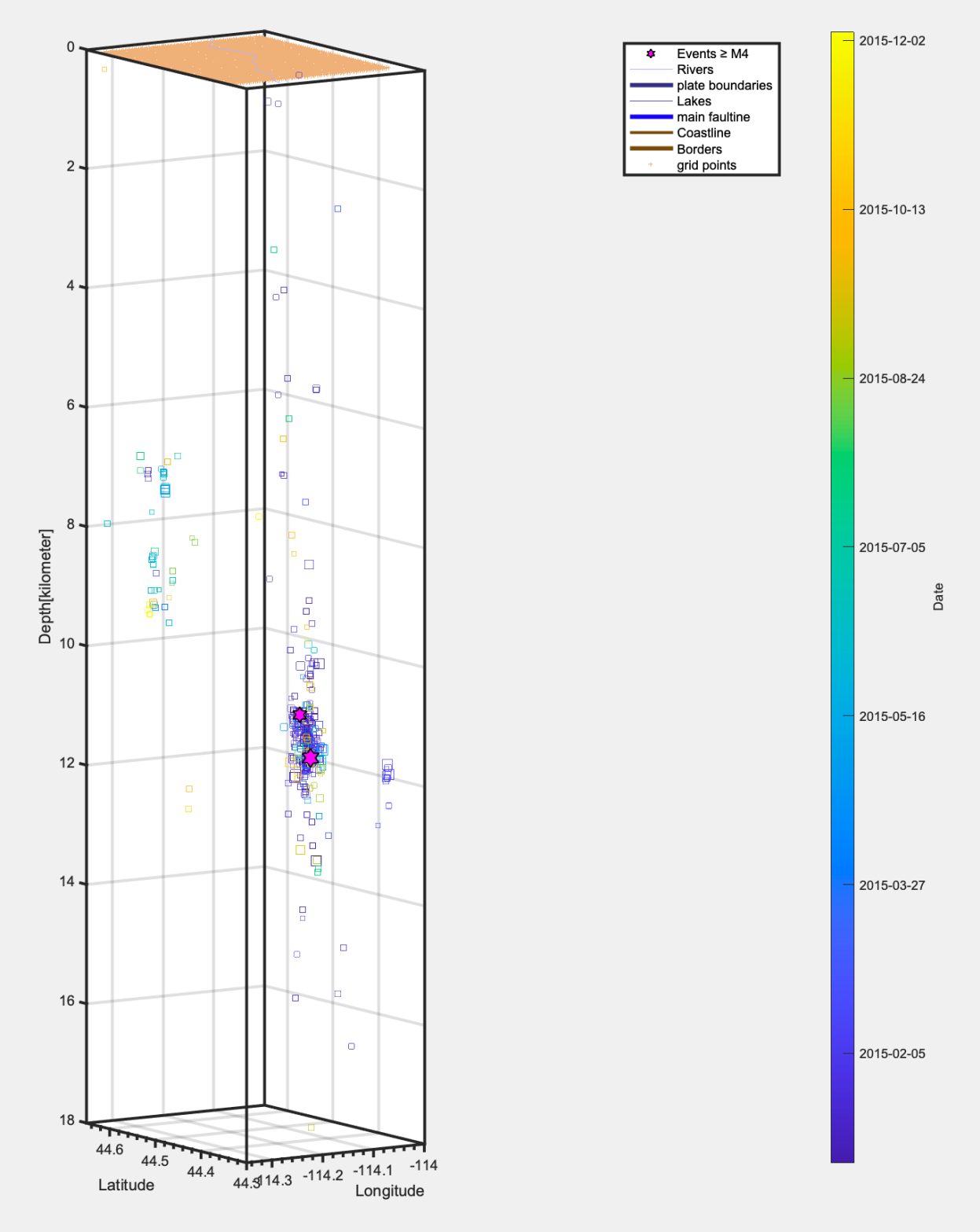

Figure 17: 3D plot of Group 2 of the Challis data, color coded for time. Stars note earthquakes M4+.

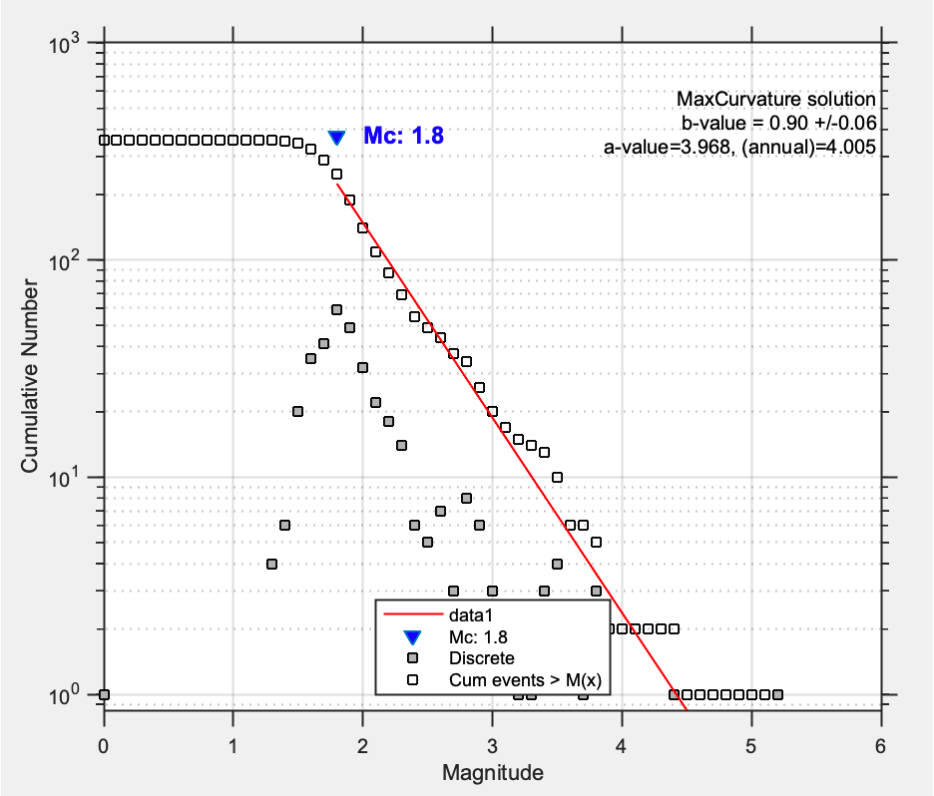

Figure 18: Frequency-Magnitude distribution of Group 2 of the Challis data.

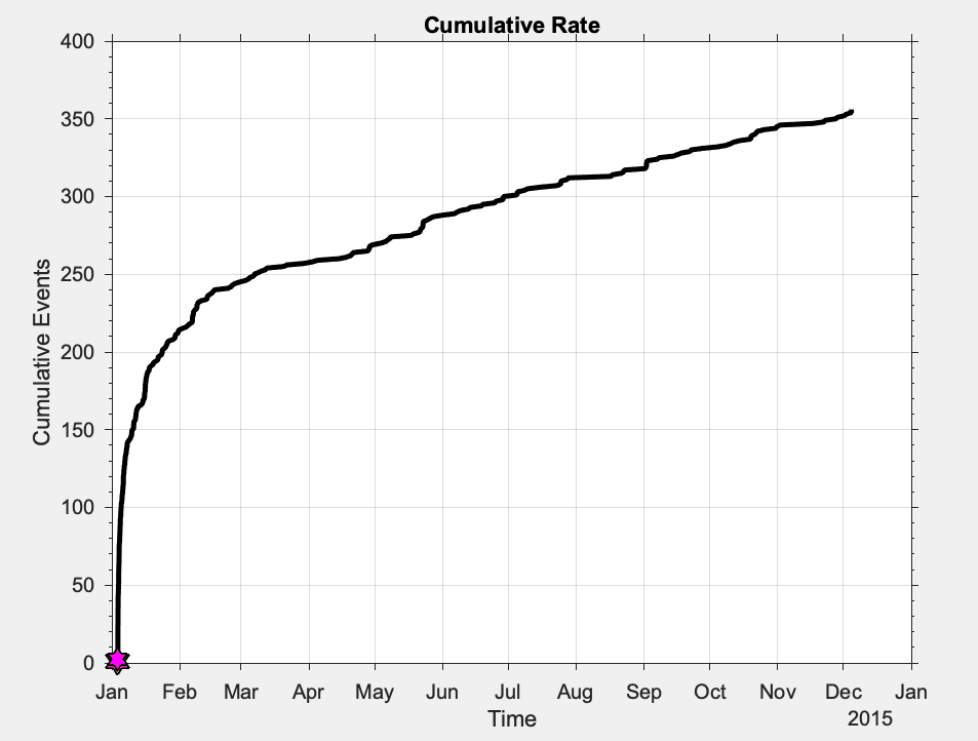

Figure 19: Cumulative earthquakes over time for Group 2 of the Challis data. Stars note earthquakes M4+.

Group 3 of the Challis data is seen in Figures 20 - 23. As seen in Figure 20, the earthquakes of group 3 occurred not only in both the northwest and southeast main clusters, but there are also minor clusters to the west and to the east of the main northwest cluster and the minor cluster further southeast of the main southeast cluster. While the minor clusters appear to occur later in this group, the earthquakes in the main clusters occur throughout this timescale, meaning there is not a significant spatiotemporal evolution in this group. Unlike the other two groups, the earthquakes of group 3 occurred over a larger range of depths, with the majority between 5 and 13km (Figure 21). Group 3 of the Challis data has a magnitude of completion of 1.7 and a b-value of 1.24 +/- 0.10, as seen in Figure 22. There is, once again, a significant stepping pattern noted in the cumulative rate plot (Figure 23), but this is not a typical mainshock-aftershock sequence. The largest magnitude earthquake in this group is a 3.6 on January 19th, 2016 and, while it occurs within the earlier part of this group, it does not occur at the beginning.

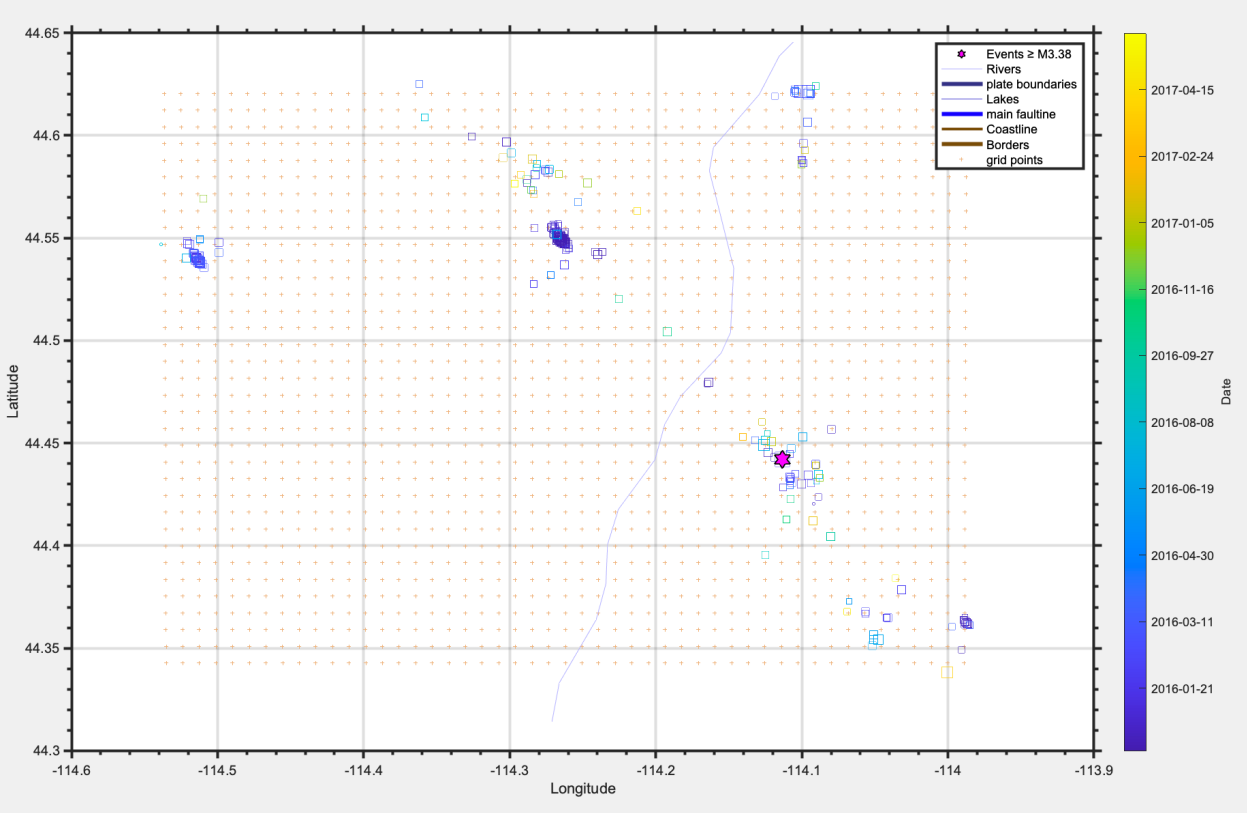

Figure 20: 2D map of Group 3 of the Challis data, color coded for time. Star marks the largest earthquake in the group, a M3.6. Blue line denotes a river in map-view.

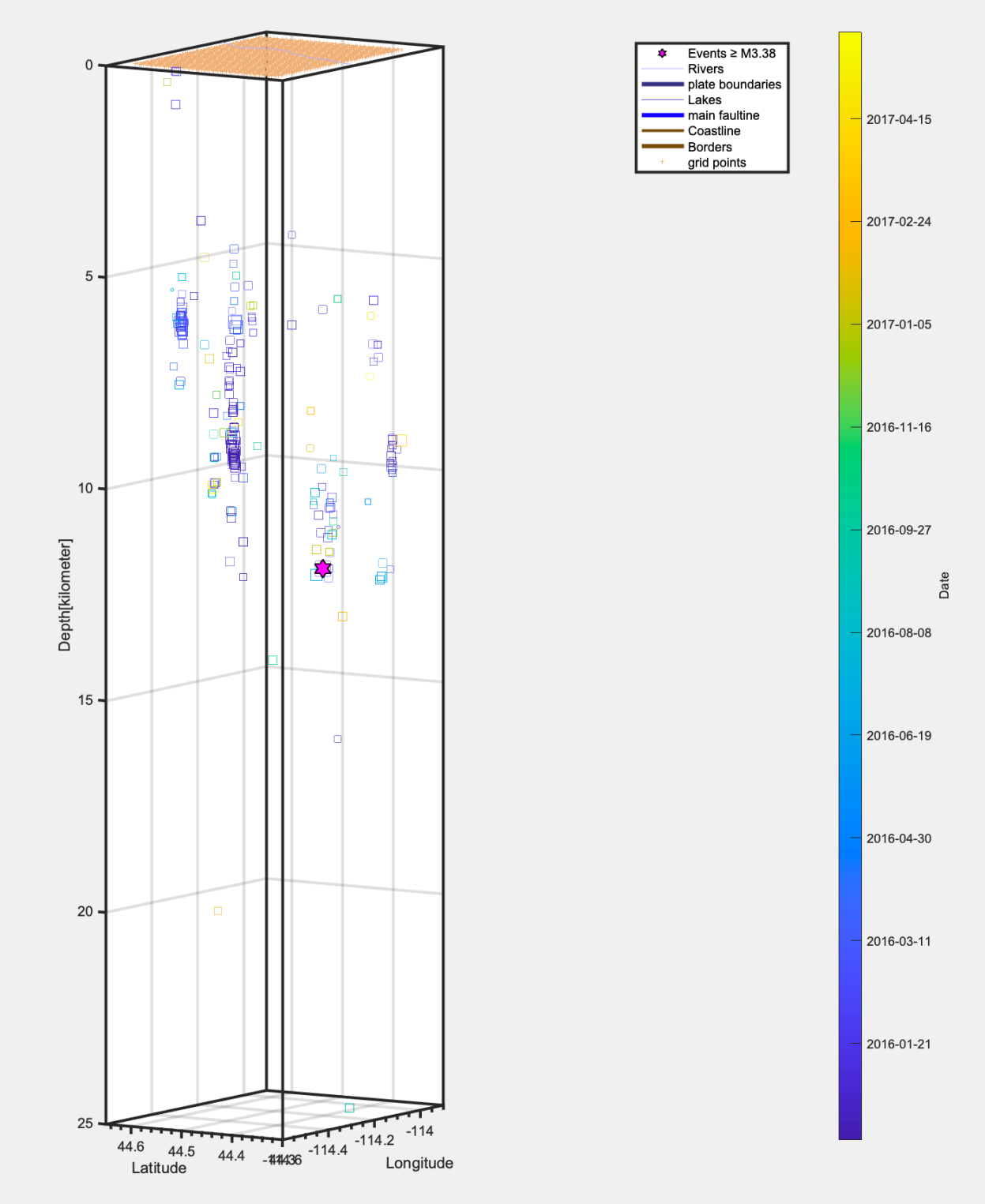

Figure 21: 3D plot of Group 3 of the Challis data, color coded for time. Star marks the largest earthquake in the group, a M3.6.

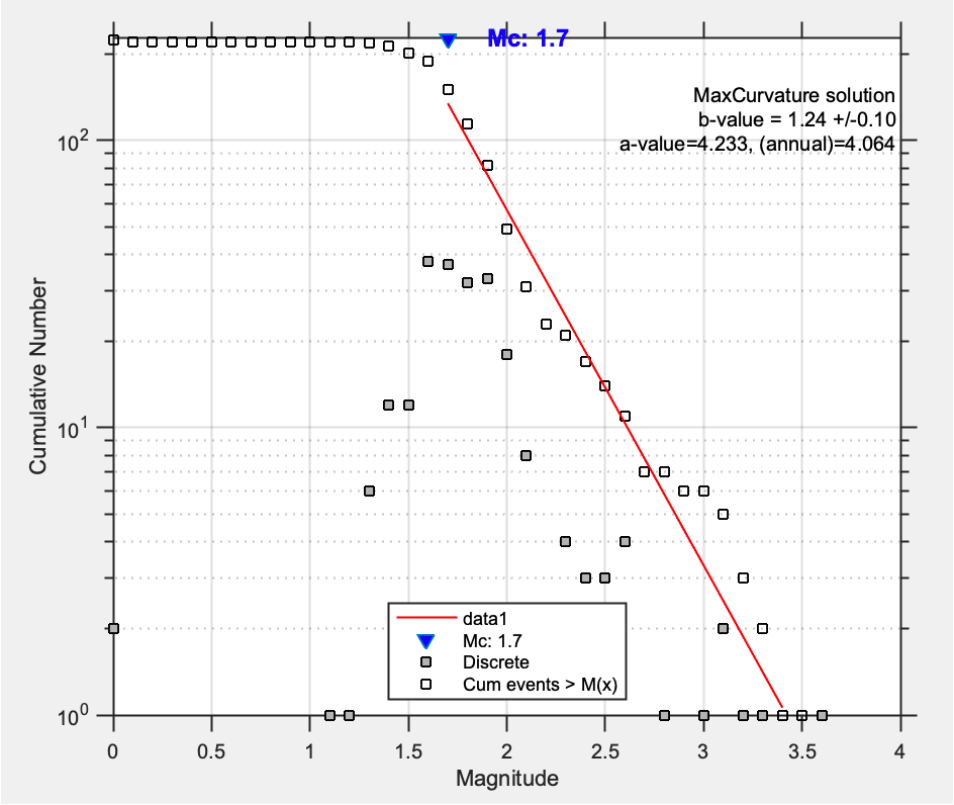

Figure 22: Frequency-Magnitude distribution of Group 3 of the Challis data.

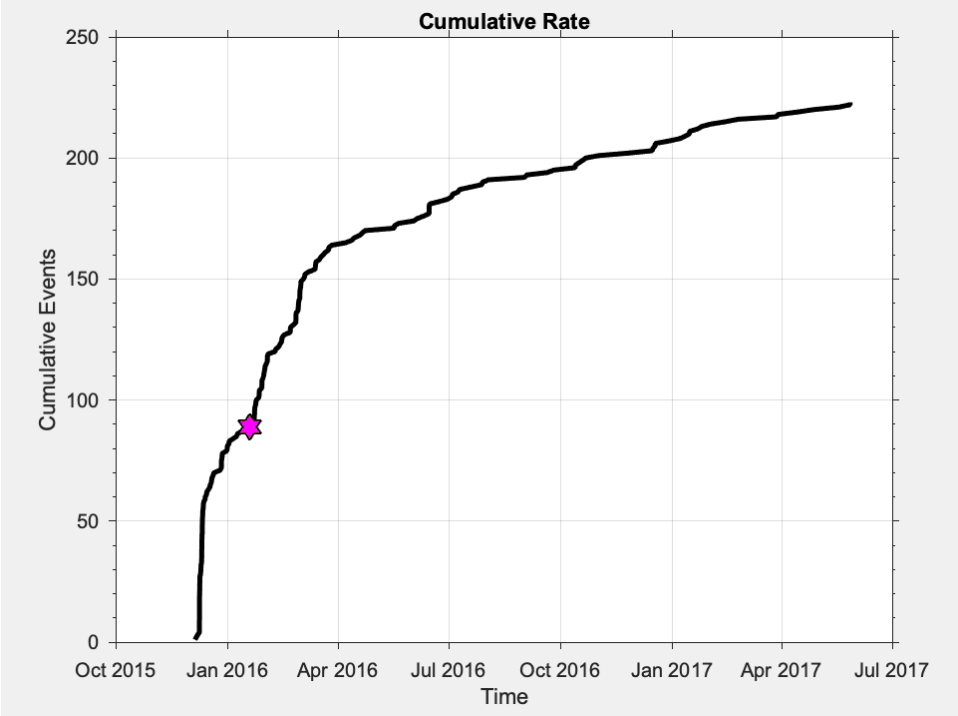

Figure 23: Cumulative earthquakes over time for Group 3 of the Challis data. Star marks the largest earthquake in the group, a M3.6.

Challis Clusters Defined Spatially

Looking at the Challis data spatially, Figures 24 - 31 focus solely on the northwest cluster. Most of the earthquakes in this cluster are also found in Group 1, the first of the three groups separated by time. As such, we once again see the five M4+ earthquakes here. There is one earthquake at about 20km depth (Figure 25), but the majority are near 10km. As the 20km depth event occurs at the end of this group, it may be part of the background seismicity that normally occurs in this area, and not part of the cluster itself. When looking at the frequency-magnitude distribution for the northwest cluster (Figure 26), it has a magnitude of completeness of 1.8 and a b-value of 0.67 +/- 0.03.

There are two significant steps in the cumulative rate plot (Figure 27). As noted previously, the earthquakes in the northwest cluster were mostly from Group 1, with some from Group 3. The Group 3 earthquakes begin on December 5th, 2015, which is consistent with the start of the second step. This northwest cluster was again split into two groups, Group A (events before December 5th, 2015) and Group B (events after December 5th, 2015). For Group A of the northwest cluster, the frequency-magnitude distribution has a magnitude of completion of 2.4 and a b-value of 0.91 +/- 0.10 (Figure 28). In the cumulative rate plot, we see a shallow step that starts about the beginning of May in 2015. There were four earthquakes between M2.8 and M3.03 that occurred at this time, which may be the reason for the shallow step, as these larger magnitude earthquakes may have produced smaller aftershocks of their own, thus increasing the number of earthquakes at that time. For Group B of the northwest cluster, the frequency-magnitude distribution has a magnitude of completion of 1.6 and a b-value of 1.13 +/- 0.10 (Figure 30). When looking at the cumulative rate (Figure 31), we see a

M3.3 earthquake represented by the star. There is little bit of a stairstep pattern here, but it also looks more or less like a main shock-aftershock sequence.

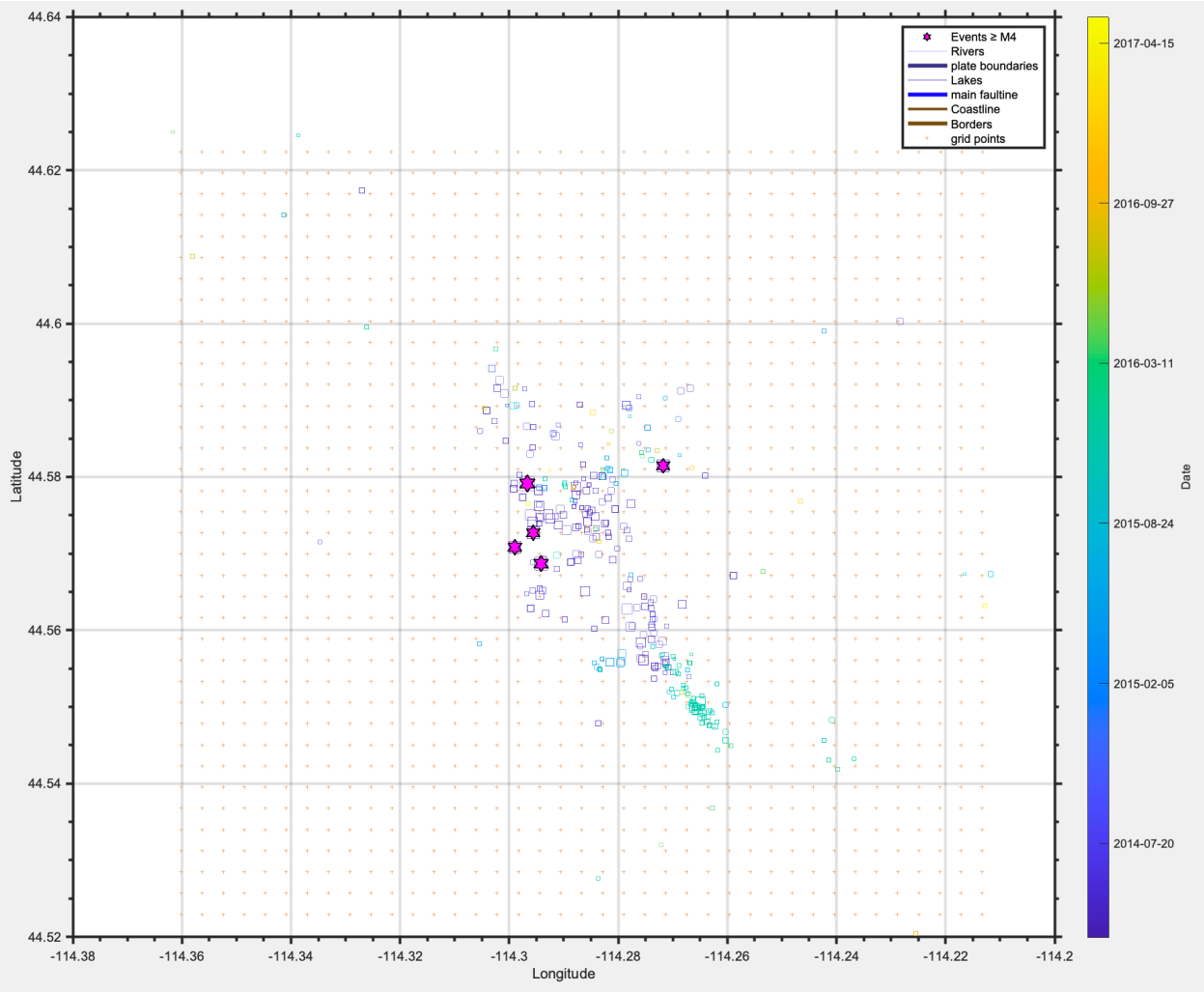

Figure 24: 2D map of the northwest cluster of the Challis data, color coded for time. Stars note earthquakes M4+.

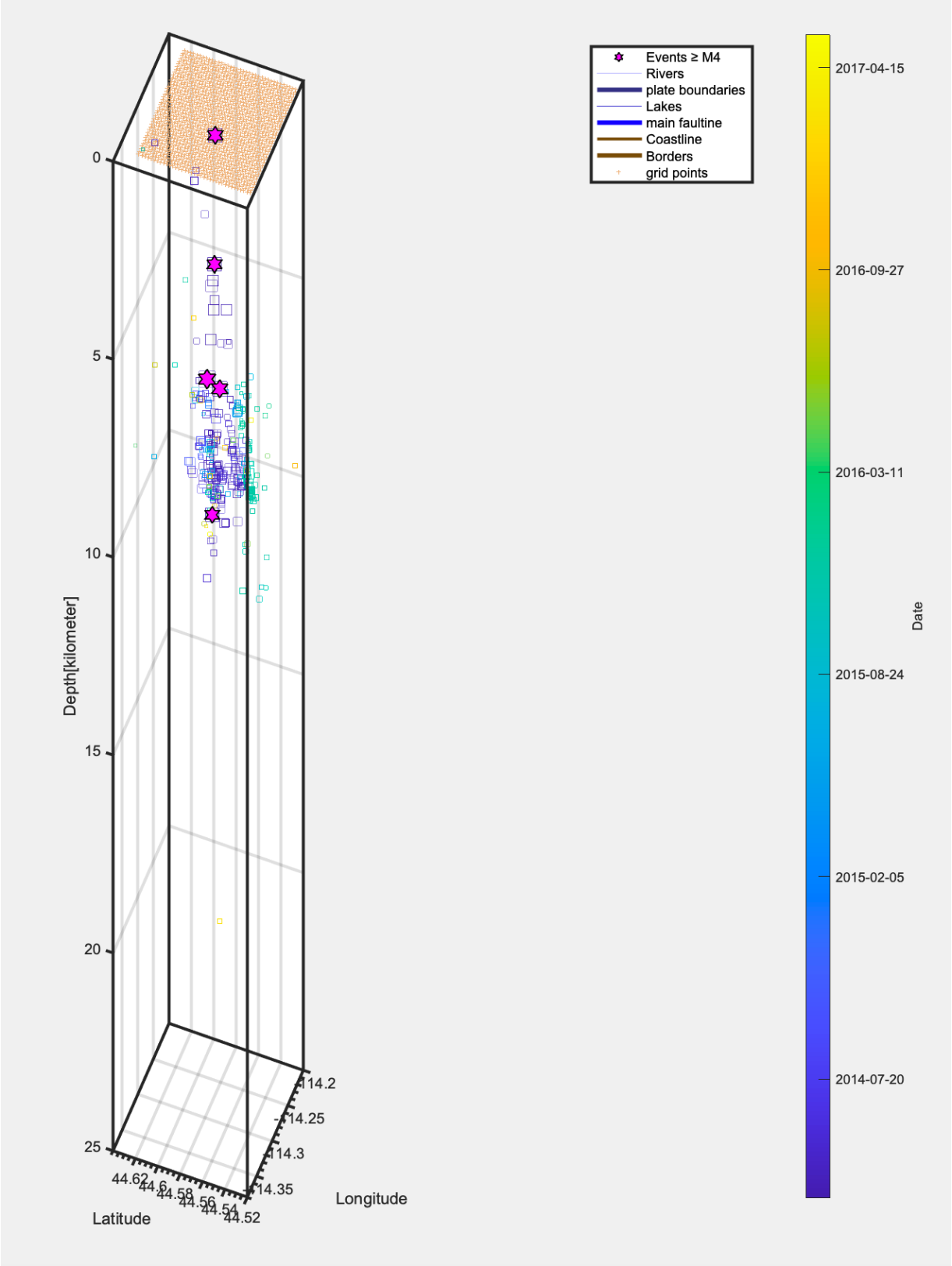

Figure 25: 3D plot of the northwest cluster of the Challis data, color coded for time. Stars note earthquakes M4+.

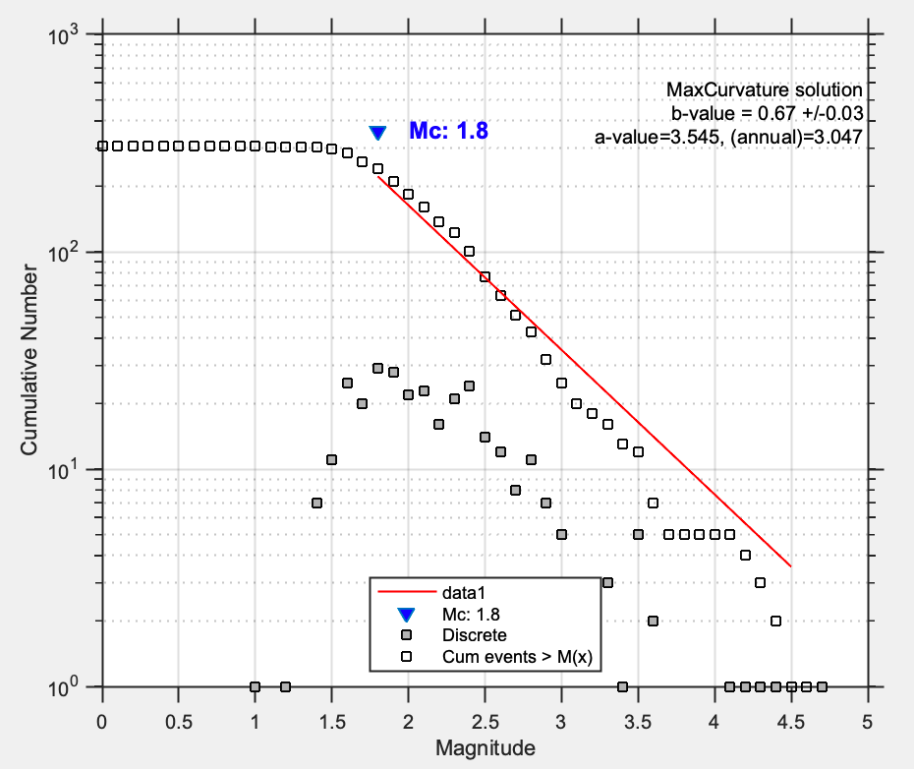

Figure 26: Frequency-Magnitude distribution of the northwest cluster of the Challis data.

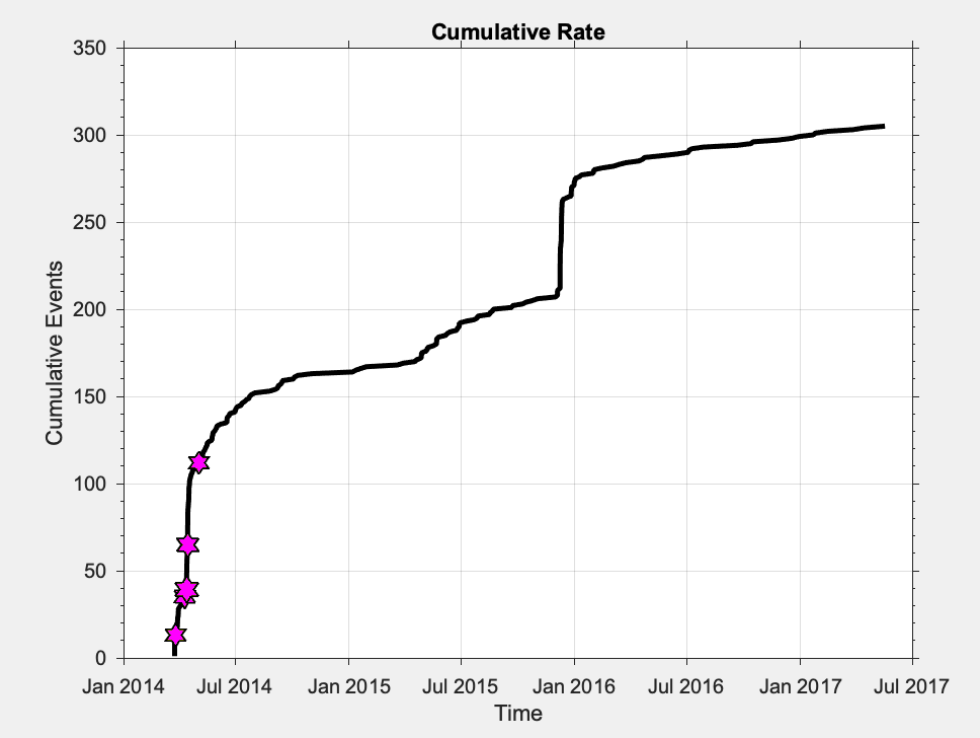

Figure 27: Cumulative earthquakes over time for the northwest cluster of the Challis data. Stars note earthquakes M4+.

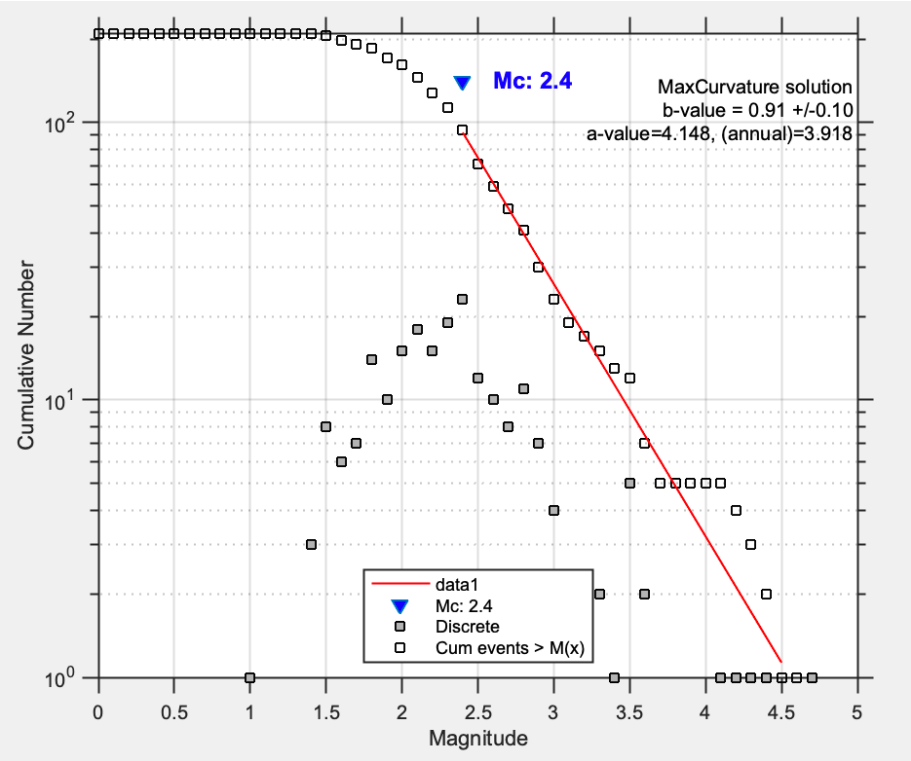

Figure 28: Frequency-Magnitude distribution of Group A of the northwest cluster of the Challis data.

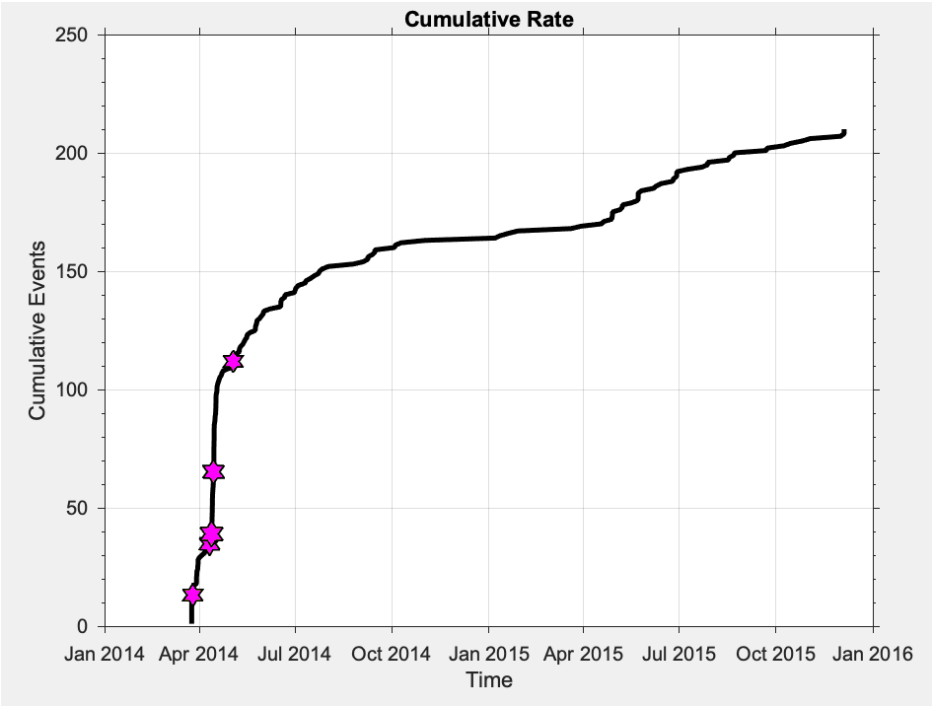

Figure 29: Cumulative earthquakes over time for Group A of the northwest cluster of the Challis data. Stars note earthquakes M4+.

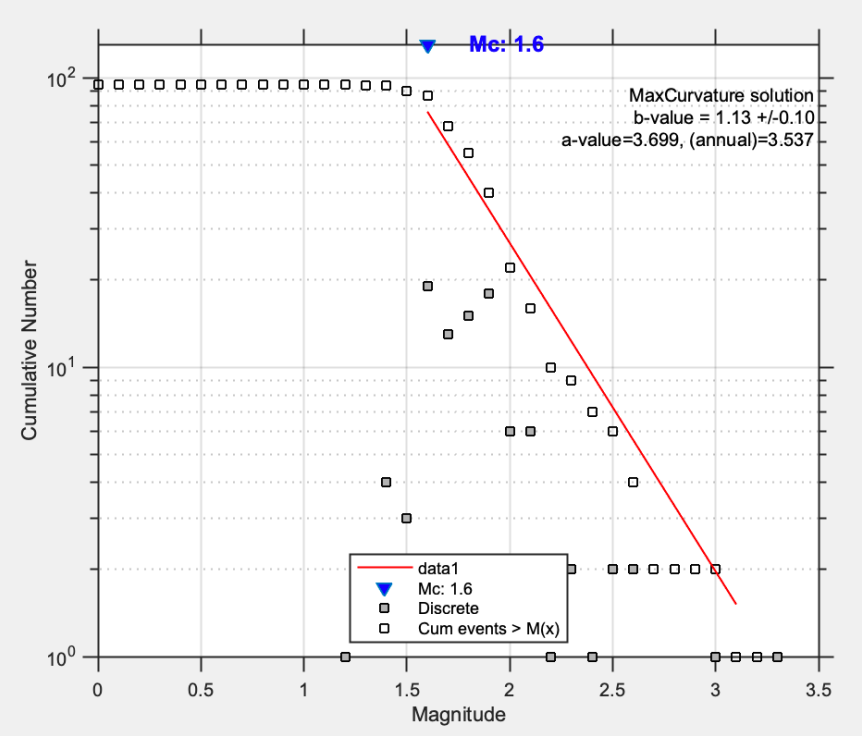

Figure 30: Frequency-Magnitude distribution of Group B of the northwest cluster of the Challis data.

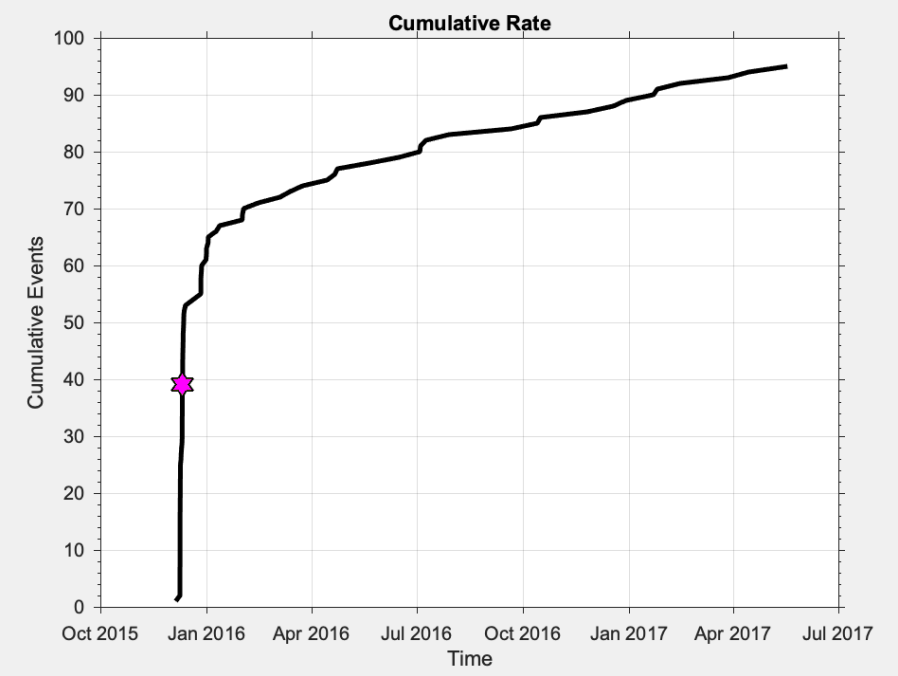

Figure 31: Cumulative earthquakes over time for Group B of the northwest cluster of the Challis data. Star marks the largest earthquake in Group B, a M3.3.

The southeast cluster (Figures 32-35) contains mostly earthquakes from Group 2, so we once again see the two M4+ earthquakes at the start of the sequence. On looking at the 3D image (Figure 33), there are a few earthquakes at greater than 15km depth, but the majority are between 10 - 13km. When looking at the frequency-magnitude distribution for the southeast cluster (Figure 34), it has a magnitude of completion of 1.8 and a b-value of 0.93 +/- 0.07. When looking at the cumulative rate (Figure 35), we see the two M4+ earthquakes represented by the yellow stars. Like the plot for Group 2, this looks like a typical main shock-aftershock sequence.

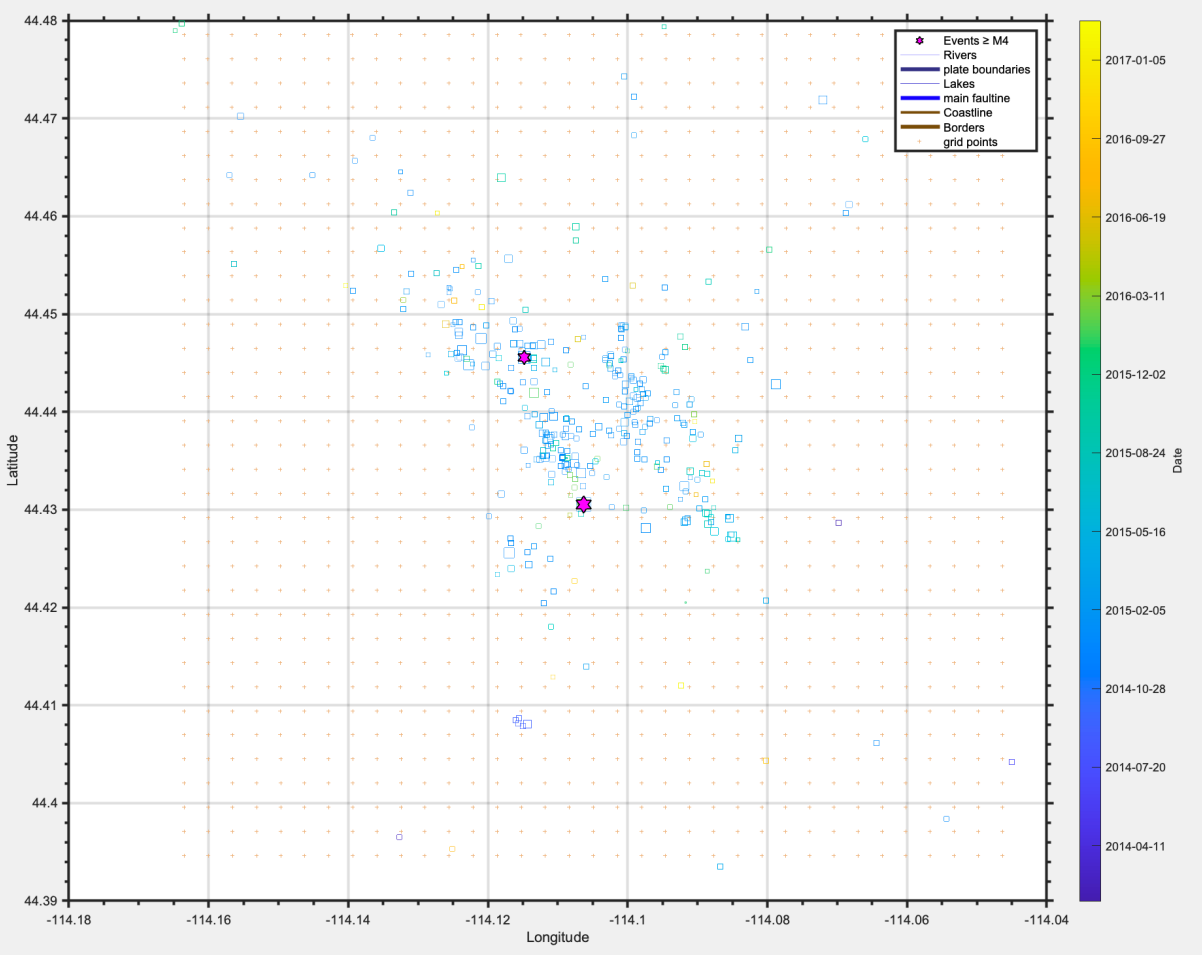

Figure 32: 2D map of the southeast cluster of the Challis data, color coded for time. Stars note earthquakes M4+.

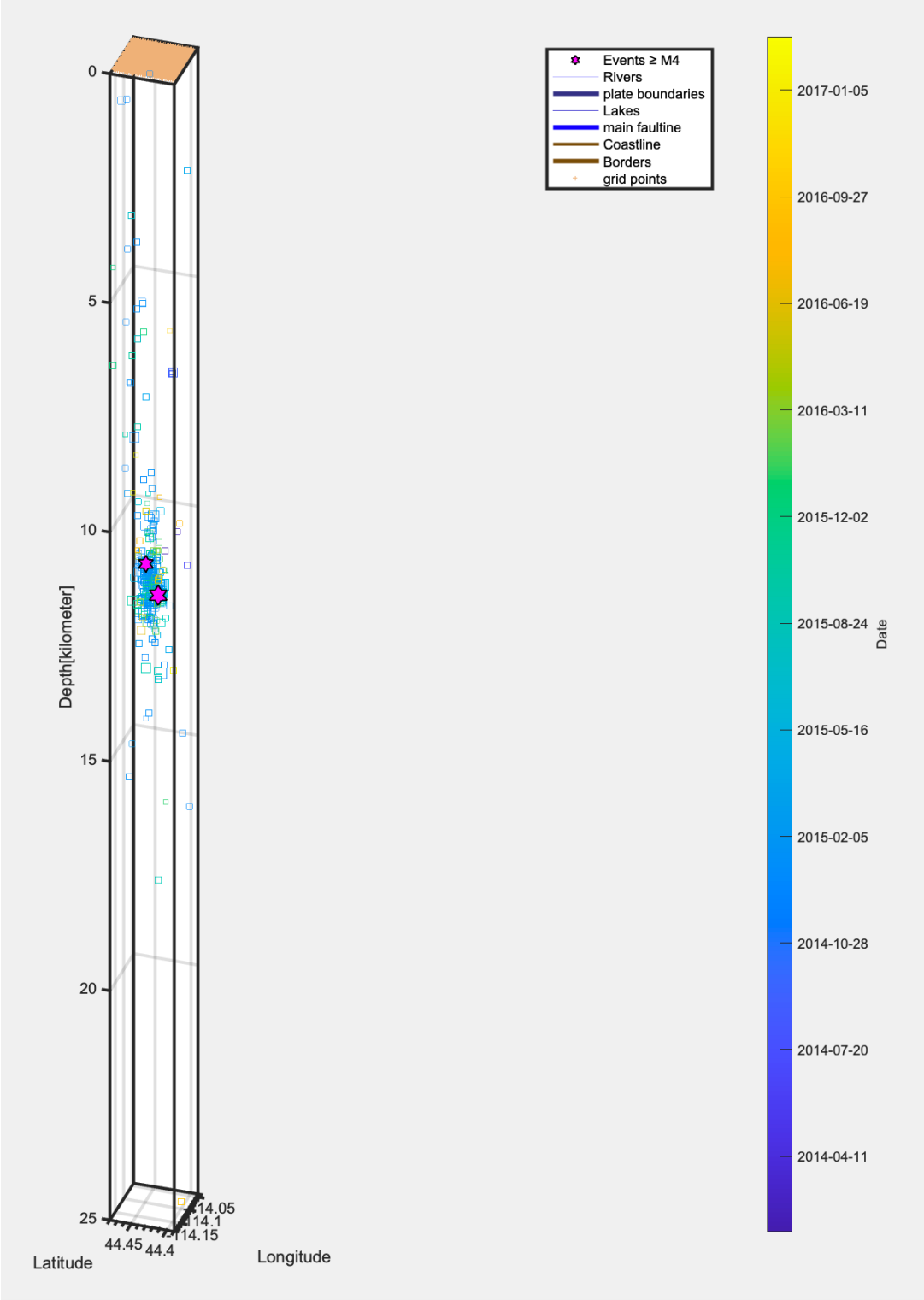

Figure 33: 3D plot of the southeast cluster of the Challis data, color coded for time. Stars note earthquakes M4+.

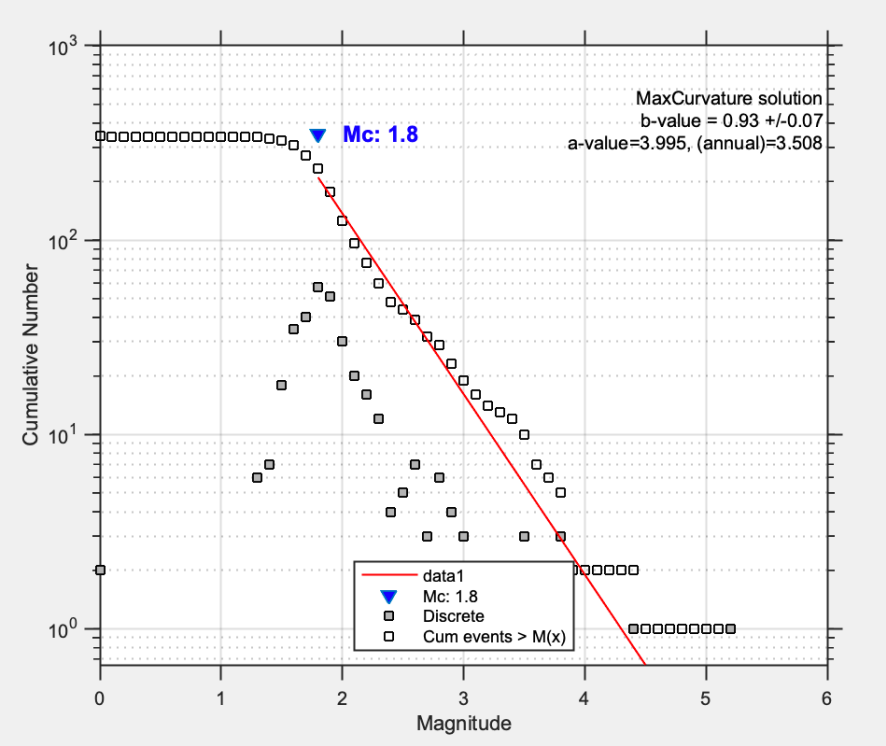

Figure 34: Frequency-Magnitude distribution of the southeast cluster of the Challis data.

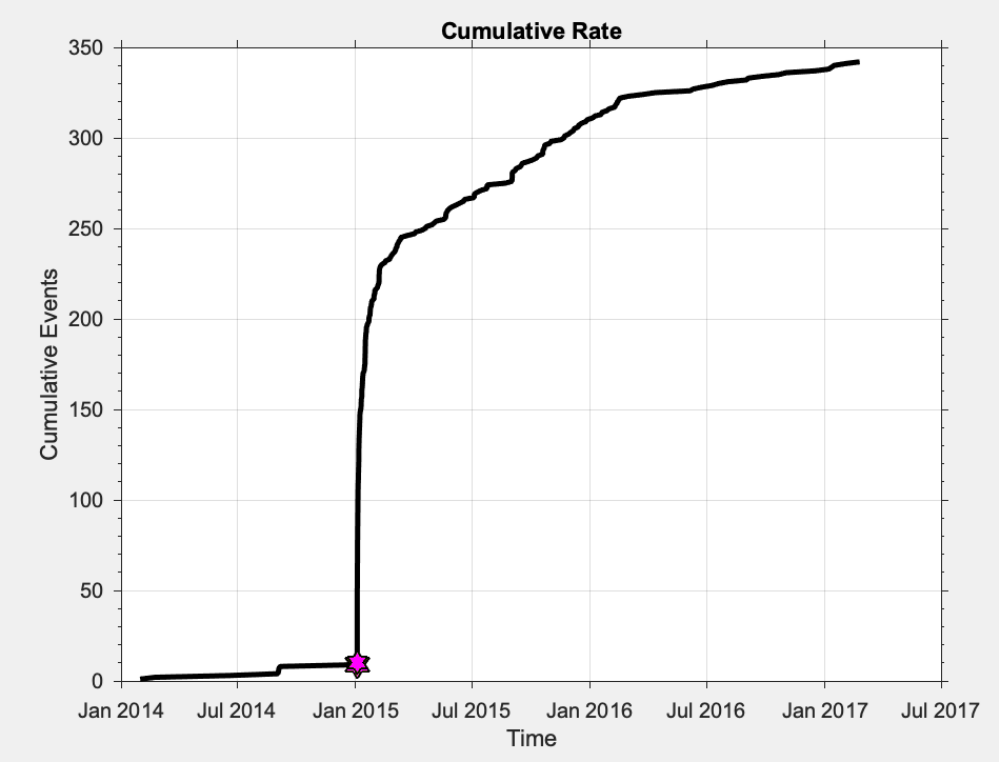

Figure 35: Cumulative earthquakes over time for the southeast cluster of the Challis data. Stars note earthquakes M4+.

When considering the Challis catalog over time via the cumulative earthquakes graph (Figure 11), there are three obvious clusters – Group 1 from January to November of 2014, Group 2 from January to December of 2015, and Group 3 from December of 2015 to May of 2017. Group 1 contains 172 earthquakes, Group 2 contains 356 earthquakes, and Group 3 contains 223 earthquakes. Pang, et al. (2018) noted two groups, earthquakes occurring in 2014 and earthquakes occurring from 2015 to 2017.

Sheldon Cluster

When looking at the catalog (USGS) for the Sheldon sequence, there does appear to be some spatiotemporal evolution, laterally from west to east, though this evolution is more obvious when considering events prior to January of 2018 (Figure 38). The depth of the majority of the earthquakes in this cluster appear to be shallower than 12km (Figure 40), and they appear to go from shallower to deeper with time. The catalog for the Sheldon cluster has a magnitude of completion of 1.4 and a b-value of 0.72 +/- 0.01 (Figure 41).

The largest magnitude events (M4.7) did not occur first, but instead at least four months into the burst, on November 6th, 2014, and September 14th, 2015. All of the events of magnitude 4.5 or greater occurred within the first 1.5 years of the burst. When looking at the cumulative number of earthquakes over time for this catalog (Figure 42), there is a slight amount of stair-step pattern. However, if only the events prior to January of 2018 are considered (Figure 43), there is a more distinct stair-step pattern likely related to the larger magnitude earthquakes at the beginning of each step.

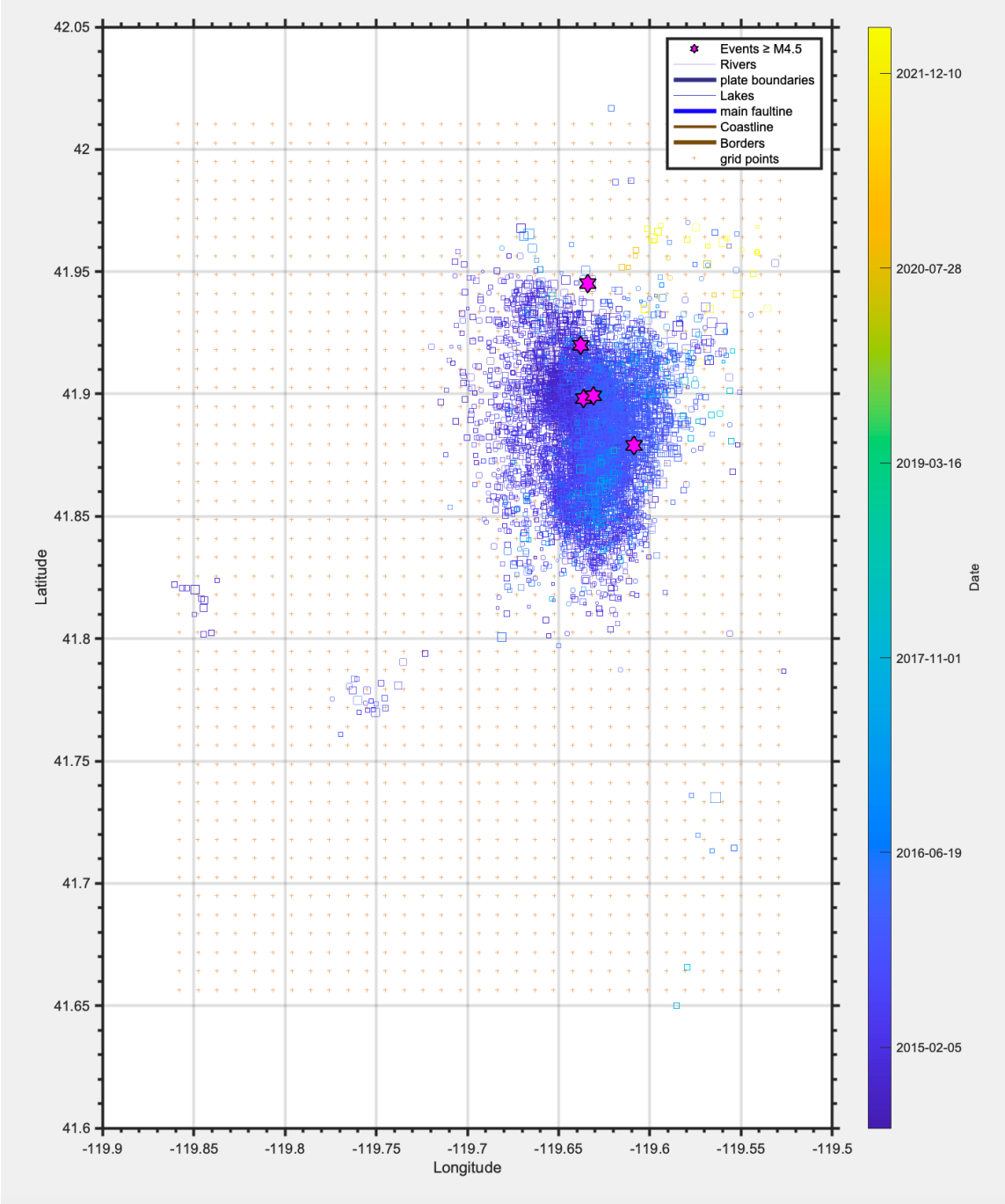

Figure 36: 2D map of the Sheldon cluster, color coded for time. Stars note earthquakes M4.5+.

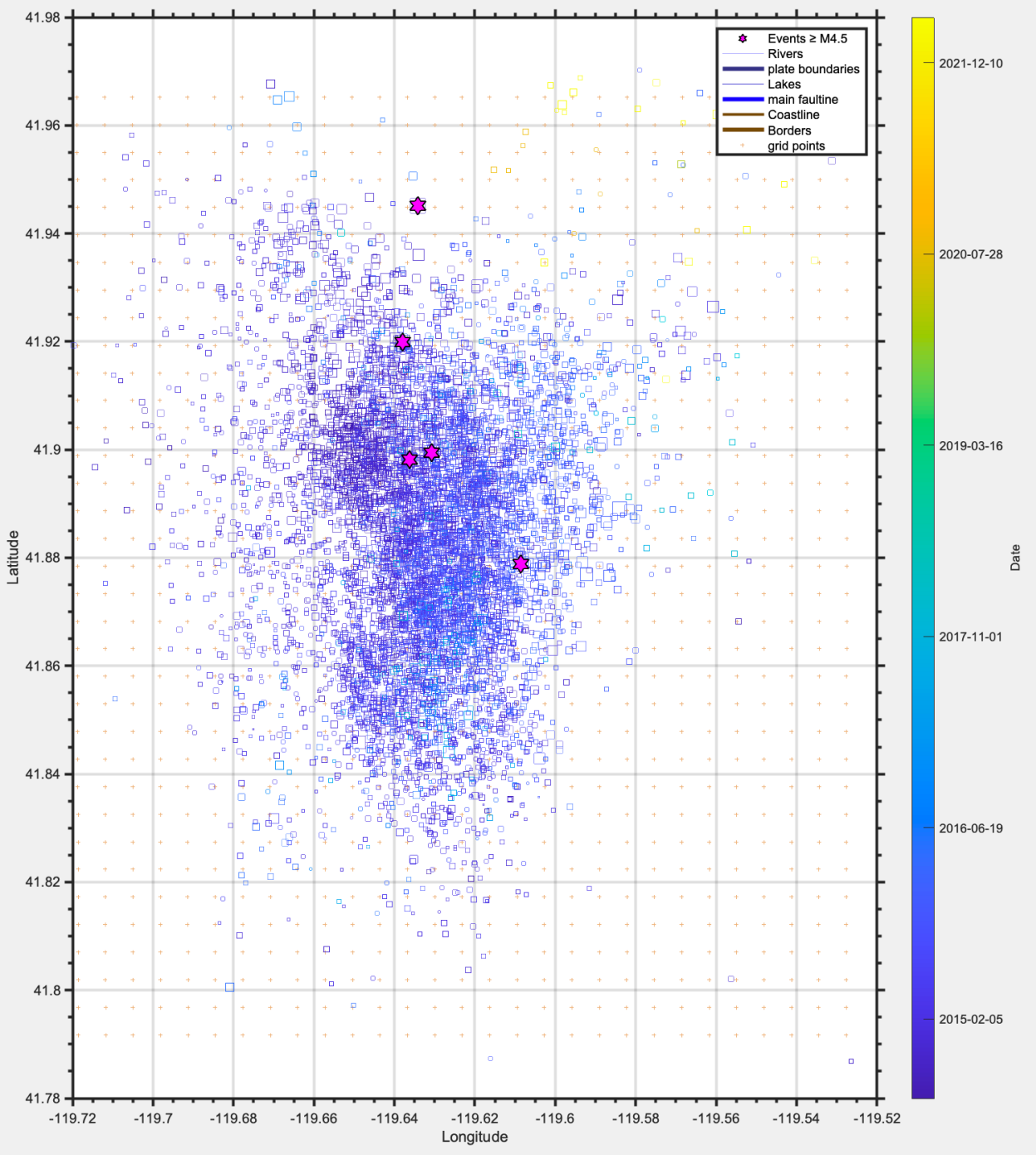

Figure 37: 2D map of the main Sheldon cluster only, color coded for time. Stars note earthquakes M4.5+.

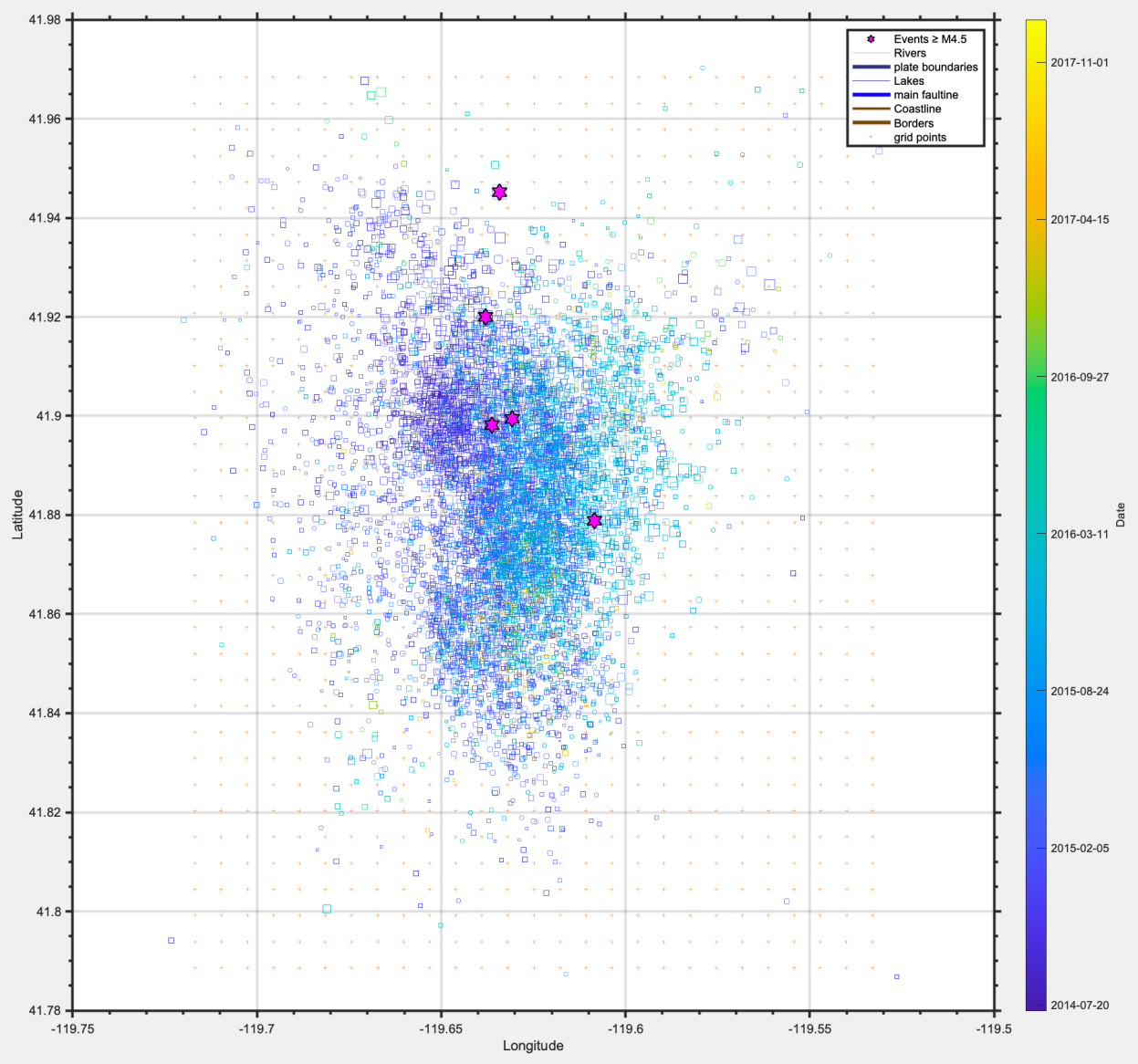

Figure 38: 2D map of the main Sheldon cluster, showing events prior to January of 2018, color coded for time. Stars note earthquakes M4.5+.

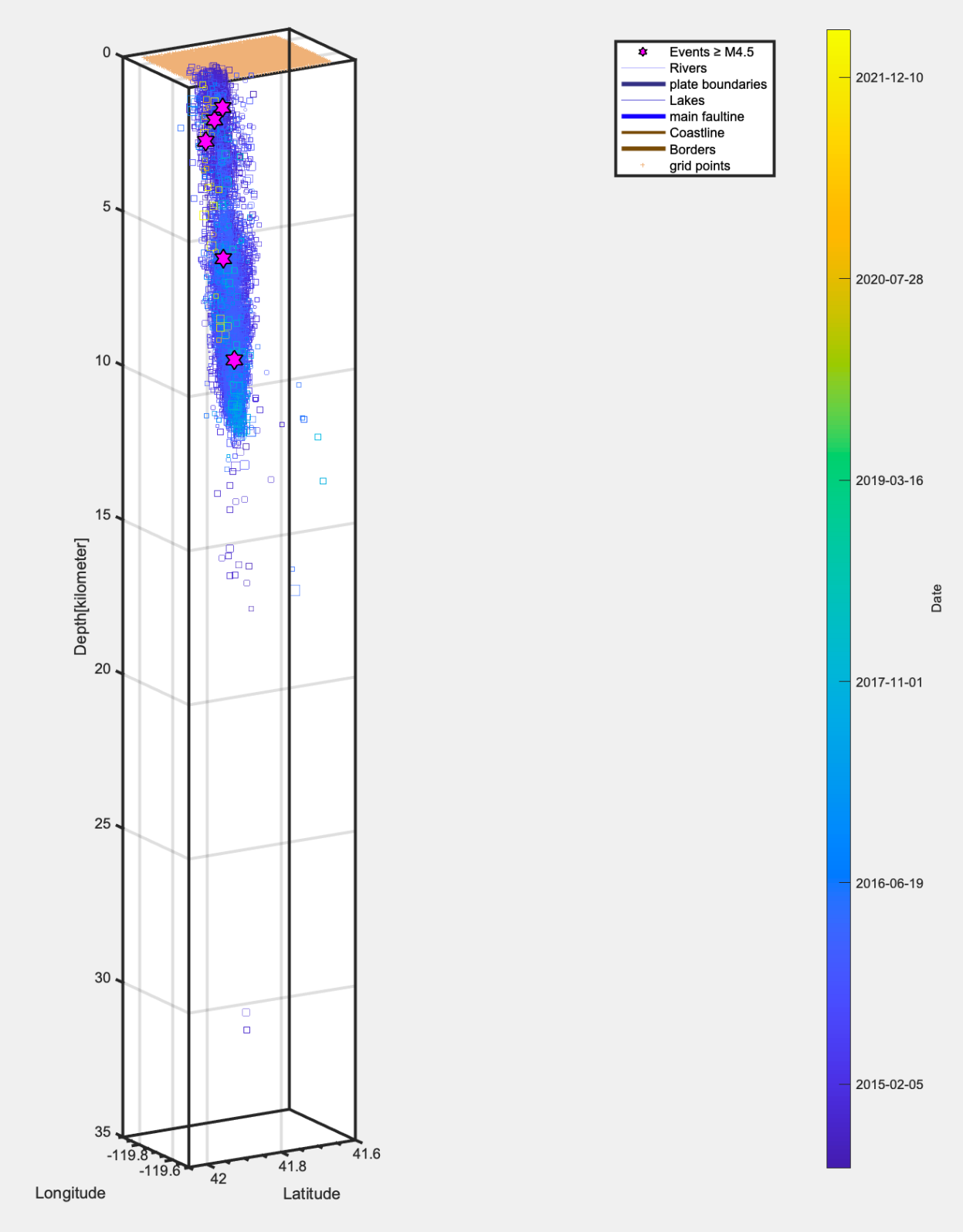

Figure 39: 3D plot of the Sheldon cluster, color coded for time. Stars note earthquakes M4.5+.

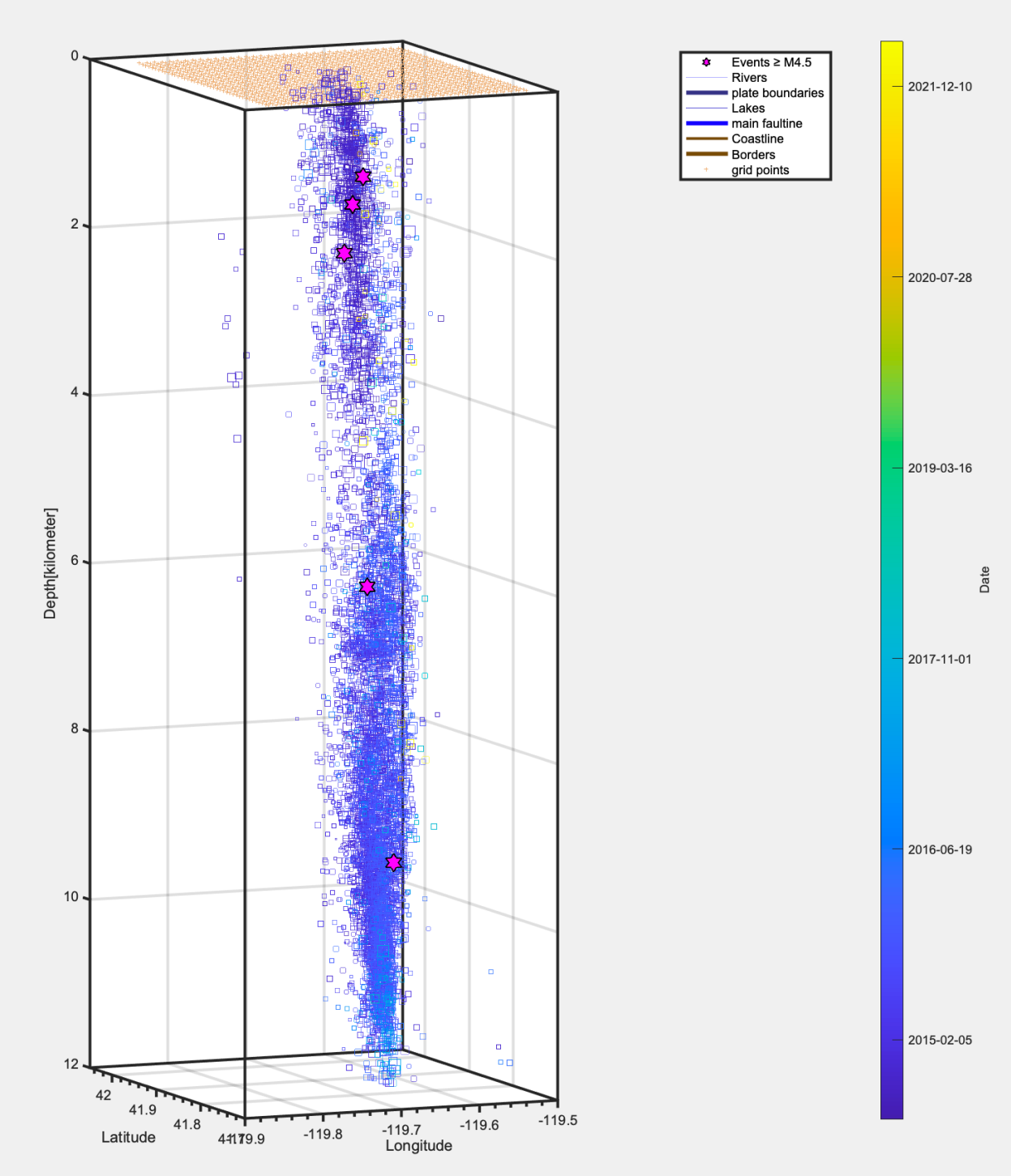

Figure 40: 3D plot of the Sheldon cluster, looking only at events at depths of 12km or less, color coded for time. Stars note earthquakes M4.5+.

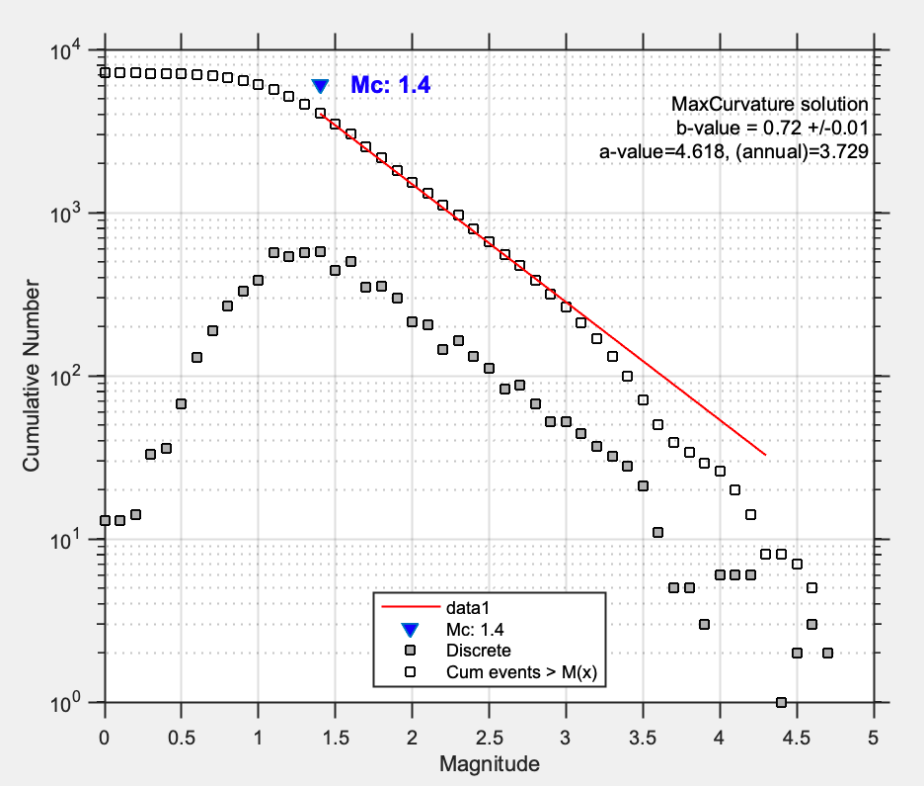

Figure 41: Frequency-Magnitude distribution of the Sheldon cluster.

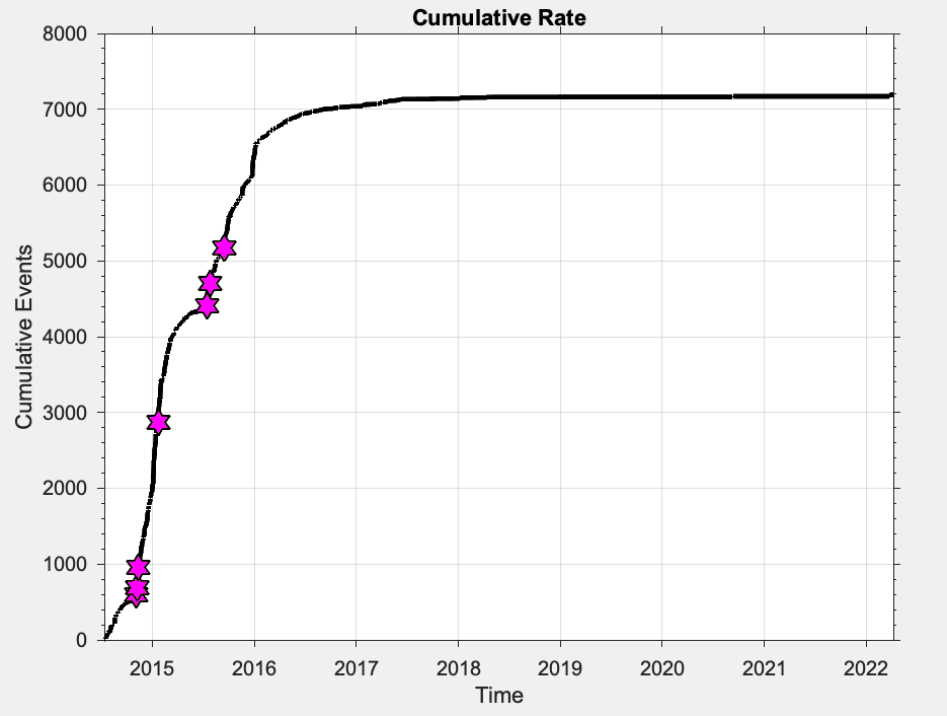

Figure 42: Cumulative earthquakes over time for the Sheldon cluster. Stars note earthquakes M4.5+.

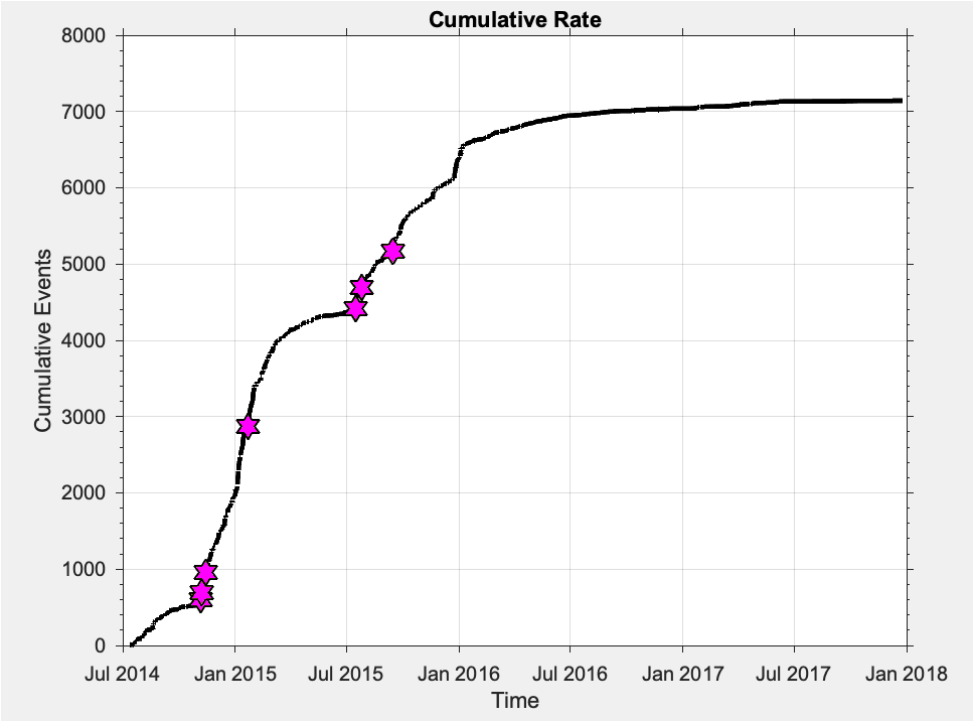

Figure 43: Cumulative earthquakes over time for the Sheldon cluster for events prior to January of 2018. Stars note earthquakes M4.5+.

Principal Component Analysis

Principal component analysis can be used to determine the shape of a seismic cluster, more specifically, the planarity, or how closely the cluster aligns to a plane. Per Vidale and Shearer (2006), the planarity of the hypocenters in a cluster is defined by $1 - \lambda 3/\lambda 2$. The eigenvalues $\lambda 1$, $\lambda 2$, and $\lambda 3$ define the principal axes for an ellipsoid that fits the seismic clusters, with $\lambda 1$ representing the longest axis and $\lambda 3$ representing the shortest axis. A value of 1 indicates that the hypocenters are all aligned on a plane and the closer the value for planarity is to 1, the closer the cluster aligns to a plane. Per Vidale and Shearer (2006), a value of 0.82 or greater is considered visually planar. Aftershock-like clusters tended to be associated with thrust faults, swarm-like clusters tended to be associated with normal faults, and both were

found to be associated with strike-slip faults. Vidale and Shearer (2006) also noted that there was not an obvious correlation between planar or nonplanar clusters and the underlying geology. For the NW Challis cluster (Table 2), the planarity is defined as 1 – 0.8437/2.3211 = 0.64. For the SE Challis cluster (Table 2), the planarity is defined as 1 – 1.0516/1.9001 = 0.45, and for the Sheldon cluster (Table 2), the planarity is defined as 1 – 3.3088/5.2335 = 0.37. Based on these results, none of the three clusters are aligned closely with a plane. However, the sparse distribution of seismometers may be a factor here. Vidale and Shearer (2006) were looking at seismic bursts in California, which has a much higher density of seismometers, meaning better coverage and a more complete catalog, thus more accurate planarity results.

TABLE 1. PCA DATA FOR THE CHALLIS AND SHELDON CLUSTERS

Eigenvalue	Results
NW Challis Cluster	
$\lambda 1$	5.2675
$\lambda 2$	2.3211
$\lambda 3$	0.8437
SE Challis Cluster	
$\lambda 1$	5.1991
$\lambda 2$	1.9001
$\lambda 3$	1.0516
Sheldon Cluster	
$\lambda 1$	14.5359
$\lambda 2$	5.2335
$\lambda 3$	3.3088

TABLE 2. PLANARITY RESULTS FOR THE CHALLIS AND SHELDON CLUSTERS

Location	Planarity Results
NW Challis Cluster	0.64
SE Challis Cluster	0.45
Sheldon Cluster	0.37

CHAPTER V

CONCLUSION

For the Challis cluster, there are several different ways to consider the data, but looking at the two spatial clusters appears to be the most logical, as the majority of the events in each cluster are also predominantly separated by time. For the northwest cluster, there is no well-defined main-shock earthquake. There does seem to be a possible spatiotemporal migration towards the southeast, which is best seen in Figure 24. The b-value is not particularly high at 0.67 +/- 0.03, which generally indicates a high stress environment (Farrell et al., 2009). However, since the b-value is slope of the Frequency-Magnitude Distribution, the b-value could also be affected by an incomplete catalog due to insufficient seismometer coverage. Although the planarity for the northwest cluster is the highest of the three analyzed, at 0.64, it still would not be considered as closely aligned with a plane. Based on the Vidale and Shearer classification (2006), the northwest cluster would fall into the "average" category. As the "average" clusters were defined as being somewhere between the other two categories and the differences between them were not always very clear, the driving force behind average bursts can vary widely. In this case, there are several active hot springs in the area and hydrothermal activity from these may play a role.

For the southeast Challis cluster, the largest magnitude earthquake (M5.2) is at the start of the sequence, making it a good candidate for a main-shock earthquake. There does not seem to be any spatiotemporal pattern, such as showing any spreading or migration. The planarity for this cluster is lower at 0.45, meaning it is not closely aligned to a plan. The b-value

is significantly higher than the northwest cluster, at 0.93 +/- 0.07. Although Vidale and Shearer (2006) noted that "aftershock-like" bursts tended to have lower b-values, the southeast Challis cluster has the largest magnitude event occurring first and it does not have a significant spatiotemporal evolution. Upon considering these factors, the southeast Challis cluster could be classified as an "aftershock-like" burst.

For the Sheldon cluster, the largest magnitude earthquake (M4.7) does not occur at the beginning of the sequence. This is a much more voluminous burst than the two Challis bursts and there is a significant lateral spatiotemporal migration from west to east. The b-value is lower, at 0.72 +/- 0.01, which would suggest a higher stress environment (Farrell et al., 2009). The planarity is the lowest of the three analyzed at 0.37, but Vidale and Shearer (2006) did acknowledge that not all swarm-like clusters aligned to planar features. The Sheldon cluster could still be classified as a "swarm-like" burst based on the larger burst volume, the significant spatiotemporal evolution, and the relatively large number of earthquakes with respect to the event of largest magnitude. Vidale and Shearer noted that the swarm-like bursts were due to underlying geophysical disturbances such as the movement of magmatic or hydrothermal fluids (2006).

The extension of the Basin and Range Province has led to both tectonic and volcanic processes occurring in this region. Therefore, it is not surprising to see clusters with different classifications located here. Due to the location of the Lost River Fault System, a result of "aftershock -like" for the southeast Challis cluster is logical and expected. A result of "swarm-like" for the Sheldon cluster would also be expected due to the lack of history of seismicity or fault systems in the area. However, the ambiguity of the "average" category leaves an

opportunity for further research. Future studies could focus on narrowing the parameters in the average category to help further understanding into the characteristics and driving forces behind these clusters. Another opportunity for future studies would involve improving the density of the seismic network in the Basin and Range Province. This would allow for better understanding of the geologically complex region.

REFERENCES

Brumbaugh, D.S., Hodge, B.E., Linville, L., and Cohen, A., 2014, Analysis of the 2009 earthquake swarm near Sunset Crater volcano, Arizona: Journal of Volcanology and Geothermal Research, v. 285, p. 18–28, doi:10.1016/j.jvolgeores.2014.07.016.

Farrell, J., Husen, S., and Smith, R.B., 2009, Earthquake swarm and b-value characterization of the Yellowstone volcano-tectonic system: Journal of Volcanology and Geothermal Research, v. 188, p. 260–276, doi:10.1016/j.jvolgeores.2009.08.008.

Konstantinou, A., and Miller, E., 2015, Evidence for a long-lived accommodation/transfer zone beneath the Snake River Plain: A possible influence on Neogene magmatism? Tectonics, v. 34, p. 2387–2398, doi:10.1002/2015TC003863.

McQuarrie, N., and Wernicke, B.P., 2005, An animated tectonic reconstruction of southwestern North America since 36 Ma: Geosphere, v. 1, p. 147–172, doi:10.1130/GES00016.1.

Moye, F.J., Hackett, W.R., Blakey, J.D., and Snider, L.G., 1988, Regional geologic setting and volcanic stratigraphy of the Challis volcanic field, central Idaho, *in* Link, P.K. and Hackett, W.R. eds., Guidebook to the Geology of Central and Southern Idaho, Idaho Geological Survey, p. 87–97.

Pang, G., Koper, K.D., Stickney, M.C., Pechmann, J.C., Burlacu, R., Pankow, K.L., Payne, S., and Benz, H.M., 2018, Seismicity in the Challis, Idaho region, January 2014–May 2017: Late Aftershocks of the 1983 Ms 7.3 Borah Peak Earthquake: Seismological Research Letters, v. 89, p. 1366–1378, doi:10.1785/0220180058.

Parsons, T.E., 1995, The Basin and Range Province *in* Continental Rifts; Evolution, Structure and Tectonics, Elsevier, 264, p. 277–324.

Payne, S.J., Zollweg, J.E., and Rodgers, D.W., 2004, Stress triggering of conjugate normal faulting: late aftershocks of the 1983 Ms 7.3 Borah Peak, Idaho earthquake: Bulletin of the Seismological Society of America, v. 94, p. 828–844, doi:10.1785/0120030122.

Richins, W.D., Pechmann, J.C., Smith, R.B., Langer, C.J., Goter, S.K., Zollweg, J.E., and King, J.J., 1987, The 1983 Borah Peak, Idaho earthquake and its aftershocks: Bulletin of the Seismological Society of America, v. 77, p. 694-723.

Ruhl, C., Bilek, S.L., and Stankova-Pursley, J., 2010, Relocation and characterization of the August 2009 microearthquake swarm above the Socorro magma body in the central Rio Grande Rift: Geophysical Research Letters, v. 37, p. n/a-n/a, doi:10.1029/2010GL045162.

USGS Earthquake Database Archives, Data for events from 2014-2018 in northwestern Nevada available at http://earthquake.usgs.gov/earthquakes/search/, last accessed July 2022.

Utsu, T., Ogata, Y., and Matsu'ura, R.S., 1995, The centenary of the Omori Formula for a decay law of aftershock activity: Journal of Physics of the Earth, v. 43, p. 1–33.

Vidale, J.E., and Shearer, P.M., 2006, A survey of 71 earthquake bursts across southern California: Exploring the role of pore fluid pressure fluctuations and aseismic slip as drivers: Journal of Geophysical Research: Solid Earth, v. 111, p. n/a-n/a, doi:10.1029/2005JB004034.

Waldhauser, F., 2001, hypoDD--A program to compute double-difference hypocenter locations: U.S. Geological Survey Open File Report 01–113.

Waldhauser, F., and Ellsworth, W.L., 2000, A double-difference earthquake location algorithm: Method and application to the northern Hayward fault: Bulletin of the Seismological Society of America, v. 90, p. 1353–1368.

Wiemer, S., and Malone, S., 2001, A software package to analyze seismicity: ZMAP: Seismological Research Letters, v. 72, p. 373–382.

Wood, C.A., 1990, Volcanoes of North America: United States and Canada (J. Kienle, Ed.): Cambridge, England, Cambridge University Press.